AFIT/GAE/ENY/92D-22

AN EXPERIMENTAL INVESTIGATION OF A
FINITE CIRCULATION CONTROL WING

THESIS

John M. Tallarovic, Captain, USAF

AFIT/GAE/ENY/92D-22

Approved for public release; distribution unlimited

AFIT/GAE/ENY/92D-22

AN EXPERIMENTAL INVESTIGATION OF A

FINITE CIRCULATION CONTROL WING

THESIS

Presented to the Faculty of the School of Engineering

of the Air Force Institute of Technology

Air University

In Partial Fulfillment of the

Requirements of the Degree of

Master of Science in Aeronautical Engineering

John M. Tallarovic, B.S.

Captain, USAF

December 1992

Approved for public release; distribution unlimited

ACKNOWLEDGMENTS

I wish to thank several individuals who made this thesis possible. Dr. Milton Franke, my advisor, challenged me with an intriguing project and supported me during the difficult times. Mr. Dave Driscroll crafted a beautiful model to test. Professor Larson provided helpful suggestions about the design of the model. Mr. Dan Riox and Mr. Andy Pitts provided outstanding technical support with the instrumentation and the wind tunnel. Most of all, I want to thank my wife, Merry, for her patience and understanding, especially at the end when things got the toughest.

Accesion For		
NTIS CRA&I		☒
DTIC TAB		☐
Unannounced		☐
Justification		
By		
Distribution /		
Availability Codes		
Dist	Avail and / or Special	
A-1		

ii

TABLE OF CONTENTS

LIST OF ILLUSTRATIONS

LIST OF TABLES

r	Coanda surface radius	(in)
R	gas constant	(lbf ft/R lbm)
Re	Reynolds number based on chord	
Re_{eff}	effective Reynolds number based on chord	
Re_{test}	test Reynolds number based on chord	
S	wing planform area	(ft^2)
t	time	(s)
T	temperature	(R)
T_{atm}	atmospheric temperature	(R)
T_t	total temperature	(R)
TF	turbulence factor	
V	velocity	(ft/s)
V_j	jet velocity of blowing air	(ft/s)
x	dimension rearward from wing leading edge	(in)
z	airfoil dimension normal to the chord	(in)

Greek Symbols

Δ	change	
γ	ratio of specific heats	
Γ	circulation	(ft^3/s)
μ	viscosity	(lb ft^2/s)
ρ	density	(sl/ft^3)

Subscripts

∞	free-stream quantity	

De	equivalent drag
e	equivalent
eff	effective
j	jet
meas	measured quantity
p	pressure
t	total property
ts	test section
1,2	station numbers

ABSTRACT

This wind tunnel investigation examined the lift, drag, and pitching moment of a 20% thick, 8.5% camber, partial elliptical cross-section, single blowing slot, rectangular, circulation control wing. The aspect ratios tested were 3.71 and 3.99. Variables included three differently shaped trailing edge Coanda surfaces and steady blowing and pulsed blowing. The test Reynolds number, based on the chord, was 500,000. The angle of attack was varied from minus 6 degrees to the inception of stall. The maximum lift coefficient measured was 3.17 with an equivalent drag coefficient of 1.85. Results also show a limit to increasing lift by increasing the blowing. Additionally, a 90 degree Coanda surface had equal lift performance and better drag performance than a 180 degree Coanda surface.

I. INTRODUCTION

High-lift devices are used by nearly all aircraft sometime during a flight. Primarily, these high-lift devices enable the aircraft to take off and land at lower speeds and in shorter distances than possible without them. Also, an aircraft using high-lift technology will be able to climb more quickly to altitude than an aircraft not employing such technology. The result from climbing quickly is a decrease in the amount of the noise reaching the ground near the airport. Vertical/Short Takeoff and Landing (V/STOL) aircraft depend on high-lift wings for their unique performance.

There are numerous practical reasons why high-lift technology is important to military applications. They include the ability to operate from runways shortened by battle damage or from short improvised runways. A given airplane re-equipped with high lift wings can carry a heavier load from the full length runway. Finally, the steeper climb possible with high-lift devices minimizes the time the aircraft is vulnerable to attack from the ground.

Currently, mechanical high-lift devices can yield high lift coefficients, but with a weight and complexity penalty. Two dimensional circulation control airfoils have been tested using blowing rates available from production engine compressor bleed. The use of circulation control tripled the lift generation of the basic airfoil section with a conventional mechanical flap.[1] The circulation control wing concept, explained in the theory section, circumvents a good deal of the mechanical complexity while still providing high lift coefficients.

With sufficient control over the blowing, this concept provides the possibility of controlling helicopter rotors without the need to change the angle of attack twice during each revolution of the rotor. The lift could be controlled by pulsing the blowing air.

One of the largest circulation control experimental efforts was conducted by Grumman Aerospace Corporation.[2] An A-6 Intruder was fitted with a circulation control wing. Lift was increased and the landing speed was decreased, but at the expense of maximum speed. The drag

of the blunt trailing edge reduced the maximum speed. The circulation control wing created such a strong nose down pitching moment that the horizontal stabilizer had to be enlarged and given inverse camber to maintain stability.

Several researchers have tested circulation control airfoils and wings in the AFIT five foot wind tunnel. Harvell[3] examined multiple blowing slots on a two dimensional airfoil. Trainor[4] and Pelletier[5] developed testing methods and tested a finite wing. Lacher[6] showed a limit on the maximum lift coefficient for a circulation control wing and began initial tests with blowing air pulsing.

This investigation had three objectives. The first was to determine if lift coefficients as high as the theoretical maximum could be obtained with a new test wing. The second objective was to test three differently shaped trailing edge Coanda surfaces and identify the best one for the given test conditions. The final objective was to test the wing with both steady and pulsed blowing and determine if wing performance was increased by pulsing the blowing air.

This investigation built upon the work of Pelletier[5] and Lacher[6]. Unique to this investigation are a new wing model of higher aspect ratio than previously tested and a new blowing air supply system. The wing was also equipped with a removable trailing edge Coanda surface. The wing was tested at a Reynolds number based on the wing chord of 500,000 in the AFIT five foot wing tunnel. The angle of attack was varied from minus 6 deg to the start of stall. Force and moment data reduced to coefficient form were obtained using a six component 0.5 in. balance and surface pressures on the wing were also recorded.

II. THEORY

According to the Kutta-Joukowski theorem, the force acting per unit length on a cylinder of any cross section is equal to:[7]

$$\vec{F} = \rho \vec{V}_\infty \times \Gamma \hat{a} \tag{1}$$

where the strength of the circulation, gamma, is defined along a unit vector $\hat{a}$ as:

$$\Gamma = \oint_C \vec{V} \cdot d\vec{s} \tag{2}$$

For a wing of span b, the total lift can be written:

$$L = \rho V_\infty \Gamma b \tag{3}$$

As the flight velocity decreases, constant lift can be maintained only by increasing any combination of the air density, the wing span, or the circulation, Γ. In practice, the most effective way to maintain lift at low airspeeds is to increase the circulation.[8]

In conventional wings, the airfoil has a sharp trailing edge. The presence of the sharp edge determines the amount of circulation about the airfoil according to the Kutta condition. The Kutta condition states that a body with a sharp trailing edge in motion through a fluid creates about itself a circulation of sufficient strength to hold the rear stagnation point at the trailing edge.[7] In contrast, circulation control airfoils have a blunt trailing edge known as the Coanda surface. Because of this blunt trailing edge, the Kutta condition does not apply. With the Kutta condition removed, the position of the rear stagnation point and the resulting circulation about the airfoil are controlled by varying the magnitude of the blowing momentum coefficient, C_μ.

$$C_\mu = \frac{\dot{m}_j V_j}{q_\infty S} \tag{4}$$

In these tests a jet of air was blown tangentially over the trailing edge Coanda surface. A balance between inertia and pressure forces keeps the jet of air attached to the curved Coanda surface for a distance. The rearward stagnation point is located where the jet separates from the

surface. By varying the strength of the blowing air, the location of the rear stagnation point, and thus the circulation, can be controlled. In this research, circulation about the wing was controlled by varying the blowing momentum coefficient.

McCormick[9] gives two limits for the maximum lift coefficient for an elliptic wing. The first is from lifting line theory and is given by: $C_{Lmax} = 1.21AR$ (5)

The second is for the exact solution for an elliptic lift distribution:

$$C_{Lmax} = 0.855AR$$ (6)

Results from this test with a rectangular wing planform will be compared to these limits.

The bulk of the tests in this research were run at a constant Reynolds number based on the model's chord of 500,000. Using the definition of Reynolds number, the definition of dynamic pressure for incompressible flow, and the equation of state, the tunnel dynamic pressure or q can be written as:

$$q_\infty = \frac{(Re\mu)^2 RT_{atm}}{P_{atm}(c)^2}$$ (7)

where atmospheric pressure and temperature are the inputs.

As shown in Equation 4, to calculate the blowing momentum coefficient, it is also necessary to know the jet velocity and the mass flow rate of blowing air. It is assumed that the air within the wing expands isentropically through the blowing slot to the free stream static pressure.[9] Starting with the following relations and the definition of Mach number:

$$\frac{T_t}{T} = 1 + \frac{\gamma-1}{\gamma}M^2$$ (8)

$$\frac{P_t}{P} = \left(1 + \frac{\gamma-1}{2}M^2\right)^{\frac{\gamma}{\gamma-1}}$$ (9)

$$M^2 = \frac{V^2}{\gamma RT}$$ (10)

The jet velocity can be solved for as:

$$V_j = \left\{ \left| \frac{2RT_t\gamma}{\gamma-1} \left[1 - \left(\frac{P}{P_t} \right)^{\frac{\gamma-1}{\gamma}} \right] \right| \right\}^{\frac{1}{2}} \tag{11}$$

where P_t is the total pressure in the wing plenum, and P is the pressure to which the jet expands. During static tests, P is the atmospheric pressure. During these wind tunnel tests, the static pressure in the tunnel test section P_{ts} is below atmospheric and is found by substituting Equation 7 for q_∞:

$$P_{ts} = P_{atm} - q_\infty \tag{12}$$

$$P_{ts} = P_{atm} - \frac{(Re\mu)^2 RT_{atm}}{2P_{atm} c^2} \tag{13}$$

The mass flow rate of blowing air was measured by a venturi mass flow meter. For this test configuration, as shown by Lacher[6], the mass flow rate is:

$$\dot{m} = C_d A_2 P_1 \sqrt{\frac{2\gamma}{RT_1(\gamma-1)}} \sqrt{\frac{1 - \left(P_2/P_1\right)^{\frac{\gamma-1}{\gamma}}}{\left(P_2/P_1\right)^{\frac{-2}{\gamma}} - \left(A_2/A_1\right)}} \tag{14}$$

where P_1 and P_2 are the pressures read at the venturi pressure taps.

Wing surface static pressure data was taken for all runs except the first run when no hoses were attached. The pressure data was reduced to coefficient form for analysis:

$$C_p = \frac{P - P_\infty}{q_\infty} \tag{15}$$

In this test, $P_\infty = P_{ts}$ and P_{ts} is simply the total pressure (or atmospheric pressure) minus the dynamic pressure. Using Equation 12 for P_{ts}, the pressure coefficient can be written instead as:

$$C_p = \frac{P - P_{atm}}{q_\infty} + 1 \qquad (16)$$

All wing surface static pressure data are presented in this form.

The drag coefficient discussed is the equivalent drag coefficient. It is used when comparing the performance of circulation control wings with conventional wings. The equivalent drag is used for comparison because it corrects for two traits unique to a circulation control wing. First, it accounts for the energy expended compressing the blowing air, the first term in Equation 17. This is energy spent by the airplane and obtained most likely in the form of compressor bleed air. Secondly, the equivalent drag accounts for the thrust caused by the jet of air exiting the wing, the second term in Equation 17. These two effects are included in two additional drag terms. As shown by Lacher[6], the equivalent drag D_e is equal to:

$$D_e = D_{meas} + \frac{\Delta KE}{V_\infty \Delta t} + \dot{m} V_\infty \qquad (17)$$

or in coefficient form:

$$C_{De} = C_D + \frac{C_\mu V_j}{2 V_\infty} + \frac{C_\mu V_\infty}{V_j} \qquad (18)$$

The free stream velocity was calculated using the definition of dynamic pressure and the equation of state.

$$V_\infty = \sqrt{\frac{2 q_\infty}{\rho}} = \sqrt{\frac{2 q_\infty R T}{P_{ts}}} \qquad (19)$$

where P_{ts} is the test section pressure. Using Equation 12 for the test section pressure, the free stream velocity is finally:

$$V_\infty = \sqrt{\frac{2 q_\infty R T_{atm}}{P_{atm} - q_\infty}} \qquad (20)$$

III. TEST EQUIPMENT

Wing Model

The wing model constructed for this test was a 20% thick, 8.5% cambered, partial elliptic cross section rectangular wing. The model had a single trailing edge blowing slot, interrupted in the center of the wing by the sting mounting block and blowing air supply tubes. Each half of the wing had a 9.0 inch blowing slot. The model could be attached to three different trailing edge surfaces. Depending on the trailing edge tested, the aspect ratio varied from 3.71 to 3.99. The wing parameters for the configurations tested are listed in Table 1.

Table 1. Summary of Wing Parameters

Trailing Edge	Chord (in)	Span (in)	Area (sq. ft)	Aspect Ratio
180	5.81	23.19	0.936	3.99
90	5.81	23.19	0.936	3.99
45	6.25	23.19	1.007	3.71

With a maximum chord of 6.25 inches, the maximum chord to tunnel height ratio of 0.104 was well below the maximum of 0.25 suggested by Wood[10] for the chord to tunnel height ratio. The airfoil geometry for the wing with the 180 deg trailing edge is given in Table 2:

Table 2. Airfoil Geometry

Surface	Coordinate (in)	Distance From LE (in)
Upper	$z = 0.28\sqrt{(2.91)^2 - (2.91 - x)^2}$	$0 \leq x \leq 5.49$
Lower	$z = -0.56\sqrt{(0.581)^2 - (0.581 - x)^2}$	$0 \leq x \leq 0.581$
Lower	$z = -0.325$	$0.581 \leq x \leq 5.49$
Coanda	$z = \pm\sqrt{(0.326)^2 - (x - 5.49)^2}$	$5.49 \leq x \leq 5.81$

7

The three trailing edges tested each had varying degrees of Coanda surface turning. The first had a 180 deg Coanda surface, typical of most circulation control trailing edges. The second had 90 degrees of flow turning, and the third had 45 degrees of flow turning. The trailing edges are referred to by the degrees of turning. In each of the trailing edges, the radius of the Coanda surface was kept the same and designed according to Englar. The Coanda surface radius to chord ratio was 0.056. The 180 and 90 deg trailing edges had the same length and resulted in a wing aspect ratio of 3.99. The 45 degree trailing edge was longer, raising the wing chord, and reducing the aspect ratio to 3.71. The three trailing edges tested are shown in Figure 1 below.

180 deg   90 deg   45 deg
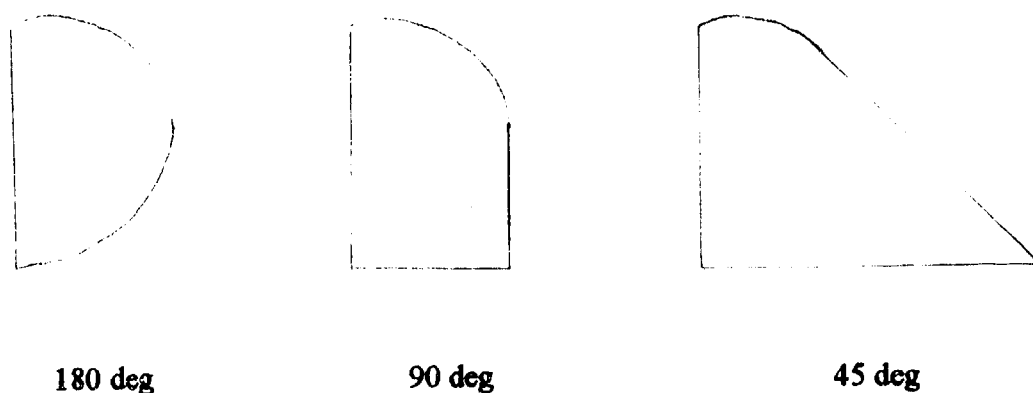
Figure 1. Cross-section of Trailing Edges Tested

The blowing air was supplied to the model by two 1/2 inch tubes exiting rearward from the wing on each side of the sting. The air supply hoses entered the wing tunnel downstream of the test section before attaching to the model. The internal flow passage of the model consisted of two independent halves, left and right, which were mirror images of each other. The interior of the model was designed as a diffuser to slow the air as much as possible to minimize pressure losses and achieve uniform distribution across the trailing edge. Within the model, the air was expanded as it flowed forward. As the air reached the leading edge, it was turned by guide vanes to flow outward toward the wing tips. The area of the duct continuously increased out to the wing tips.

8

Turning vanes were used to turn and distribute the air uniformly across the slot at the trailing edge, Figure 2.
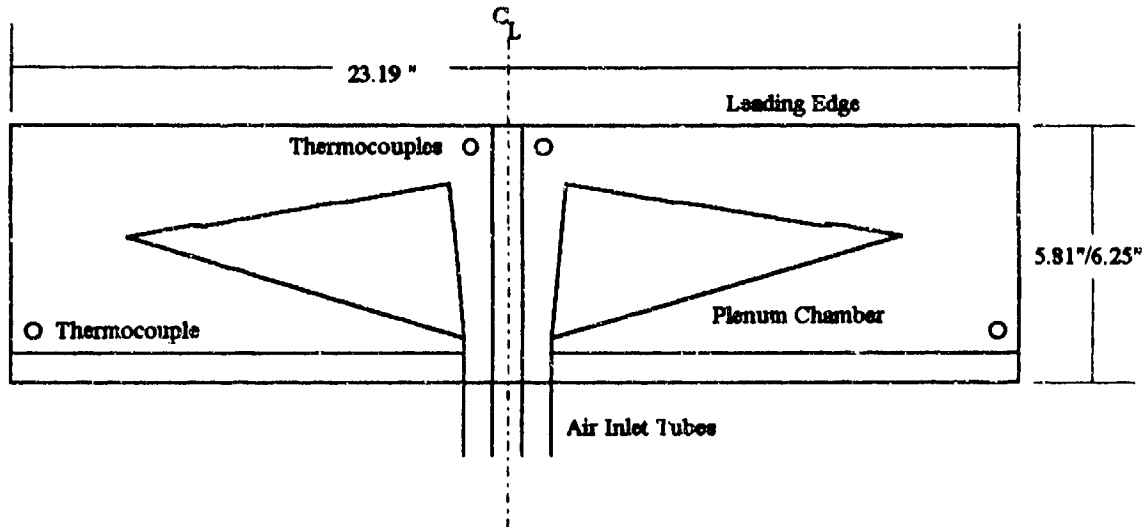
Figure 2. Planform View of Test Wing

The height of the trailing edge slot where the blowing air exited could be varied by 14 adjustment screws on the upper surface. When tightened, the screws brought the upper surface down and closed the blowing slot. The slot height was typically 0.009 in, giving a slot height to Coanda radius h/r=0.028. Englar[1] suggests that strongly attached Coanda flow is maintained for $0.01 \leq h/r \leq 0.05$.

The model contained a total of 71 pressure ports. Two were used to measure the total pressure in the plenum on each side of the wing. The remaining 69 were static pressure ports on the surface of the model. Table 3 shows the chord locations of the surface mounted pressure ports.

Table 3. Wing Static Pressure Port Locations

6 inches from left wing tip		6 inches from right wing tip	
Upper	Lower	Upper	Lower
x/c	x/c	x/c	x/c
0.000	0.017	0.000	0.098
0.024	0.048	0.100	0.207
0.048	0.095	0.308	0.306
0.095	0.203	0.510	0.408
0.201	0.305	0.709	0.504
0.306	0.403	0.940	0.608
0.406	0.501	0.969	0.704
0.511	0.604	0.991	0.809
0.609	0.701	1.000	0.907
0.709	0.804		0.940
0.801	0.902		0.969
0.940	0.940		0.991
0.969	0.969		
0.991	0.991		
1.000			

The flow temperature within the model plenum was measured by four thermocouples. The thermocouples were positioned in pairs, two in each half of the wing. One pair was located in the front of the model near where the flow entered, and the other pair was positioned near the trailing edge. The thermocouples were required to determine the velocity of the jet of air exiting the model. Also, the pairs of thermocouples within the same side of the wing were used to check for temperature changes in the air as it flowed through the model.

Blowing Air Supply System

Blowing air for the test wing was supplied by a Kaeser compressed air system. The system consisted of a Kaeser CS-90 compressor capable of delivering 360 cfm at 110 psi, a 200 gallon tank, a Kaeser refrigerated type compressed air dryer, and an in-line oil filter. After exiting the compressor, the air flowed through the settling tank, drier, and filter in turn before being directed

to the wind tunnel control room. The compressor was set to maintain 110 psig +/- 3 psi in the tank. The blowing air supply system is shown in Figure 3.

| Compressor | — | 200 gal Tank | — | Drier | — | Filter | — | Wind Tunnel Control Room |

Figure 3. Blowing Air Supply System

Within the control room, the compressed air flowed through a valve, cyclone separator, and filter before it was used. Next, the model pressure was controlled by a regulator. For these tests, the air flow for each test run was set using the regulator. To measure the mass flow of blowing air used, a thermocouple and a venturi mass flow meter followed the regulator. Beyond this location, two different air routes were used, depending on whether steady or pulsed blowing was used. For the steady flow tests, the air was divided into two streams, one for each half of the model, and routed into the tunnel test section, Figure 4.
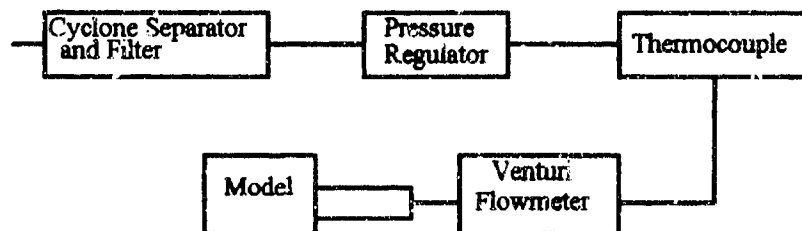
Figure 4. Blowing Air Supply System for Steady Blowing Tests

A schematic of the pulsed blowing system is shown in Figure 5. In these tests, the air was divided into two streams following the venturi mass flow meter. One of the streams entered the pulser valve, and the other served as a bypass. A gate valve was used to control the amount of bypass flow. The bypass air mass flow was measured by a second venturi mass flow meter. Downstream of the bypass flow meter the pulsed air was introduced, allowed to mix, and again divided into two streams for each half of the model. The bypass air was required to moderate the

severity of pressure fluctuations entering the model. Earlier tests passed all the blowing air through the pulser valve and the resulting lift oscillations seriously damaged the model.[6]
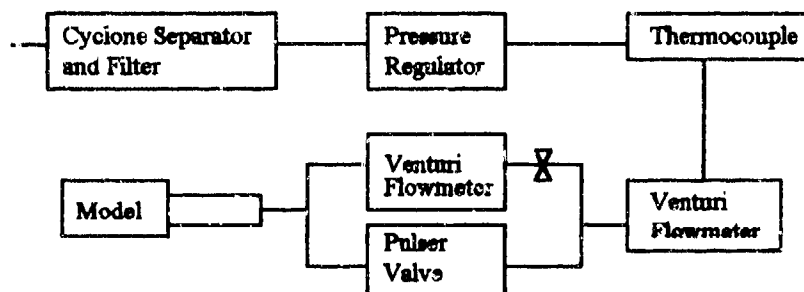
Figure 5. Blowing Air Supply for Pulsed Blowing Tests

The pulser valve used in these tests was the same as used by Lacher. The rotary pulser valve had a cylindrical brass core with two perpendicular air passages in it. The core was spun within a steel housing having the inlet and exit ports. Because of the two air passages, there are four pulses of air for each revolution of the valve. The pulser valve was driven by a direct current motor with a speed controller. A counter was used to determine the pulsing frequency.

AFIT 5-ft Wind Tunnel

All tests were performed in the AFIT 5 foot wind tunnel at Wright-Patterson Air Force Base. The open circuit tunnel has a closed test section and is enclosed in a building designed specifically for the tunnel. The entrance has a contraction ratio of 3.7 to 1 and the test section is 5 feet in diameter. Tunnel airspeeds up to 200 mph are provided by two counter rotating 12 foot fans driven by four DC motors.

The total pressure in the tunnel is assumed to be atmospheric and the static pressure is measured by a ring of eight static pressure ports located 2.5-ft from the tunnel mouth. Tunnel dynamic pressure (tunnel q) is taken as the difference between atmospheric pressure and tunnel static pressure. To maintain a constant Reynolds number throughout testing with changing atmospheric conditions, a new tunnel q was calculated prior to each run.

The wind tunnel has a turbulence factor (TF) of 1.5. When comparing test results from different wind tunnels, the effective Reynolds number, as defined below, is used.

$$Re_{eff} = TF \times Re_{test} \qquad (21)$$

where Re_{test} is the test Reynolds number. The effective Reynolds number is higher because it accounts for the additional turbulence in the wind tunnel caused by the propeller, the guide vanes, and the vibration of the tunnel walls.[11]

Data Acquisition System

The data acquisition process was controlled by a Zenith Data Systems Z-300 computer using the AFIT 5 foot wing tunnel data acquisition and reduction software. Data acquisition was also partly controlled by a Hewlett-Packard 3852A Data Acquisition Control Unit (DACU) which read outputs from the sting balance, angle of attack potentiometer, tunnel temperature thermocouple, tunnel q pressure transducer, and the model base pressure transducer.

Forces and moments on the model are measured by an Able Corporation Mark V balance. The 0.5-in diameter, six-component, strain gauge balance measures two normal forces, two lateral forces, one axial force, and one rolling moment. Pitch and yaw moments were resolved by using the two normal and two side force measurements. Excitation voltage was provided by a Hewlett Packard 6205 regulated power supply. Output voltages were read by the DACU and stored in the Z-300. After completion of a run, the voltages were converted into forces during data reduction using the calibration matrix.

Several different pressure measurements were made during testing. They included: static pressures on the surface of the wing, total pressures of the blowing air inside of the wing, static pressures at the venturi meter taps and time varying pressures during pulsed testing.

The static pressures on the wing surface and the total pressures in the wing plenum were measured with a Pressure Systems Inc. 780B/T Pressure Measurement System Data Acquisition and Control Unit using a 780B/T Pressure Calibration Unit. The pressure transducers were

13

housed in Electronically Scanned Pressure (ESP) sensors. The pressure measurement system was connected to the HP 3853A DACU with an IEEE-488 interface bus. For this test, a +/- 45 psia ESP sensor and a +/- 5 psig ESP sensor were used. The ESP units were attached through 3/32 inch tubing to the model pressure ports and mounted in the wind tunnel downstream of the test section. The control and calibration units for the ESP units were located outside of the wind tunnel. The pressure measurements were coordinated with the rest of the measurements by the DACU.

The model base and the tunnel q pressures were measured with two Robinson-Halpern 0-25 inches of water pressure transducers. Two venturi flow meter pressure measurements were made using Endevco 8530A-100 pressure transducers powered by Endevco 4225 power supplies and conditioned with Endevco 4423 signal conditioners. The output voltages were read with standard voltmeters. Two other venturi flow meter pressure measurements were made with a 50 inch Mercury manometer.

A pressure transducer was mounted in the blowing air supply line to measure the shape of the pressure pulse entering the model during pulsed testing. Two locations were chosen for measurements. The first measured the pressure just past the mixing of the pulsed and bypassed air. The second was located about 12 feet downstream in one of the blowing air supply lines approximately 1.5 inches from the model. For the second measurement, the transducer was located as close as possible to the model so that the wave form of the pressure entering the model could be determined. The pressure was measured with an Endevco 8530A-100 pressure transducer powered by an Endevco 4225 power supply and conditioned with an Endevco 4423 signal conditioner. The output voltage was read on a Tektronix 7854 recording oscilloscope.

IV. EXPERIMENTAL PROCEDURE

Calibration

The sting balance was calibrated prior to any testing by loading each of the strain gauges of the Mark V balance with known loads. With the exception of the axial force gauge, all gauges were loaded in the positive and negative directions of the balance's coordinate system. Since only positive axial forces were expected, that gauge was only calibrated in the positive direction. Each normal force gauge was calibrated using a 20 point calibration from 0 to 50 lbf, each side force gauge was calibrated using an 18 point calibration from 0 to 50 lbf, and the rolling moment gauge was calibrated with a 12 point calibration from 0 to 10 lbf.

During the calibration of any one gauge, the wind tunnel DACU recorded the applied load, all strain gauge voltages, the sting angle of attack, and the sting bend. After completion of the calibration for each gauge, a calibration file was written for that gauge. The linear fit of the calibration file was checked with the correlation coefficient. All of the gauges had a correlation coefficient of 0.99996 or greater. The process was repeated for each gauge in the positive and negative directions where applicable. After the 11 calibration files were collected, they were combined into a single calibration matrix. The calibration matrix included any cross-talk between the gauges when loading occurred. The calibration matrix was used during testing to reduce the raw gauge voltages into forces and moments.

During the calibration, a sting bend file was written for each gauge relating the applied load to sting bend. This file was used later during data reduction to correct the angle of attack measured with the potentiometer for the deflection of the sting due to aerodynamic loads.

Before testing, the angle of attack voltage was related to the wing angle of attack. The wing was mounted on the sting with an inclinometer to measure the angle of attack. The wing was set at a given angle and the voltage recorded. This alpha-voltage schedule was used to set the wing angle of attack while the tunnel was running and for the DACU to determine the angle of attack.

The three Endevco pressure transducers were calibrated prior to testing with an Ametek dead weight tester using 19 and 15 point calibrations. The Robinson-Halpern transducers were also calibrated with an Ametek dead weight tester using a 25 point calibration. For all pressure transducers, the calibration curve correlation coefficient was 0.999 or greater.

Test Item Checkout

The jet velocity across the trailing edge slot was checked for uniformity prior to the model entering the tunnel. It was important that the velocity and mass flow of blowing air out the blowing slot be uniform across the span of the wing to achieve consistent and repeatable performance during testing. The model was mounted on a table with the blowing air hoses attached and a total pressure probe was positioned in the jet of air exiting the wing. Jet total pressure measurements were made in 0.5 inch intervals along the span of the wing. Also, the total temperature within the wing, and the ambient pressure were recorded. From these, the jet velocity was calculated using Equation 11. The slot height was adjusted to achieve a even flow velocity distribution across the span as possible. The best flow was achieved when the slot height was uniform across the span. Therefore, when the model was in the tunnel only the slot height needed to be checked. The maximum variation in jet velocity within any side was 12% and a typical jet velocity survey is shown in Figure 6.
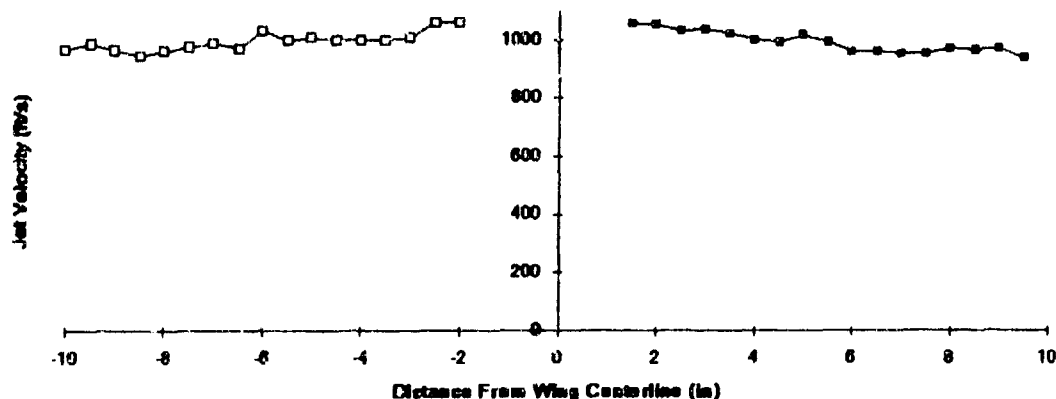

Figure 6. Velocity Profile at Trailing Edge

After the model was installed in the tunnel and all the data acquisition channels connected, several test runs were performed before the wind tunnel was started. To determine if installation of the model disturbed the main balance, the model and balance were loaded with a check load. Measurements from the balance within 3% of the applied load were determined to be acceptable.

Testing

In this test program, a run consisted of an angle of attack sweep with the other parameters held constant. The angle of attack was varied in 2 deg increments from -6 deg to the start of stall (between 14 and 22 deg). The Reynolds number based on the wing chord was 500,000 for nearly all tests. A new q was calculated, using Equation 7, prior to each run using current atmospheric conditions. The parameters varied were the trailing edge Coanda surface shape, the amount of blowing air (represented by the blowing coefficient), and whether the blowing air was steady or pulsed. In the pulsed tests, an additional variable was the pulsing frequency.

Following the initial tare, the wing was tested without hoses attached. After another tare with the hoses attached, testing of the trailing edges began. This was done to isolate any effect the hoses may have on the forces and measured. Next, the thrust of the jet of air at three values of the blowing coefficient was measured with the tunnel off. Finally, the wing was tested with the tunnel running at the same three blowing coefficients. With this method, the contribution of the jet of air can be isolated from the lift coefficient in the reduced data. Steady blowing was used for these tests. The same general procedure was followed for all the trailing edges tested.

The 180 deg trailing edge was later reinstalled for a hysteresis check. In all of the testing to this point, the angle of attack increased from -6 deg to the final value. For the hysteresis check, the angle of attack was decreased from the maximum value to minus 6 deg and compared to a previous run where the angle of attack increased.

Pulsed testing followed the steady blowing tests. The variables for the pulsed tests were the angle of attack, the blowing coefficient, and the frequency of the pulsing. All pulsed tests were

performed with the 180 deg trailing edge. Three angles of attack were examined: -2, 0, and 2 deg. The frequency of the pulsing was varied from zero (steady blowing) to 80 Hz.

Figures 7 and 8 show two views of the model mounted in the tunnel test section. In Figure 7 the 3/32 inch surface pressure lines are visible entering the ESP units mounted on the sting. Figure 8 shows the two 1/2 inch blowing hoses entering the rear of the model.

Figure 7. Model in Tunnel Test Section Looking Downstream
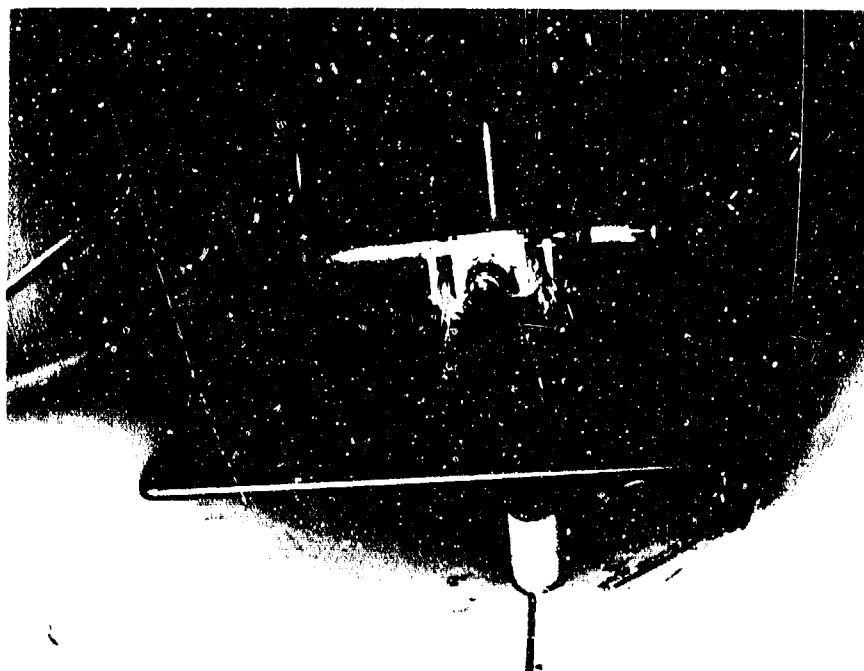
Figure 8. Model in Tunnel Test Section Looking Forward

The pulsed blowing air plumbing is shown in Figure 9. Visible are the thermocouple used to measure the incoming flow temperature, the two venturi flow meters, and the by-pass valve. The pulser valve and it's motor are in Figure 10.

Figure 9. Blowing Air Instrumentation

Figure 10. Pulser Valve and Drive Motor

V. DATA REDUCTION

Wind Tunnel Corrections

Raw data from the wind tunnel main balance was first reduced by the wind tunnel data

acquisition system software into the measured force and moment coefficients. All of the force and

moment data were reduced in the wind axis where lift is perpendicular and drag is parallel to the

undisturbed flow. While the coefficients were being calculated, several standard wind tunnel

corrections were applied as recommended by Pope.[11] The corrections applied included: skew

factor correction to q, solid blockage correction to q, wake blockage correction to q, wind tunnel

buoyancy correction to the drag coefficient, induced drag correction to the drag coefficient, base

pressure correction to the drag coefficient, and an up-wash correction to the angle of attack. Table

4 lists the corrections and their relative size for a typical test run. The corrections applied to the

tunnel dynamic pressure were all very small. The drag coefficient corrections were much larger in

comparison and the angle of attack correction was very small. In addition to the wind tunnel

corrections, the following additional corrections, unique to this investigation, were applied: lift

coefficient corrections, drag coefficient corrections, and pitching moment corrections.

Table 4. Summary of Wind Tunnel Corrections

Correction	Percentage of Final Value
Skew Factor, q	1.9
Solid Blockage, q	0.10
Wake Blockage, q	0.11
Buoyancy, Cd	11.8
Induced Drag, Cd	12.6
Base Pressure, Cd	19.1
Up wash, Alpha	0.3

Lift Coefficient Corrections

The lift coefficient had two corrections applied: the first for the effect of the blowing hoses and another for the component of lift caused by the thrust from the jet of blowing air. The first correction was obtained by plotting lift coefficient versus alpha for the wing without and with the blowing hoses attached, Figure 11.
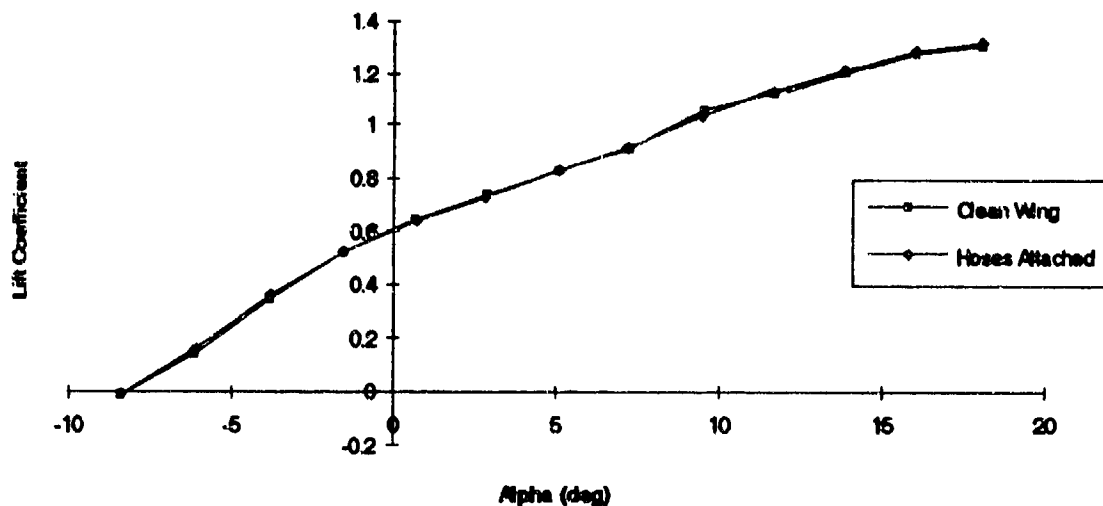
Figure 11. Effect of Blowing Hose on Lift Coefficient

Each lift coefficient curve in Figure 11 was fitted by a second order polynomial. Since the two runs were completed at identical conditions, the difference between the curves was due to the presence of the blowing hoses. The correction for the blowing hoses was equivalent to the difference between the two curves. The correction, a function of the angle of attack, was calculated for every lift coefficient measurement based on it's corresponding angle of attack. This correction was then added to all measured values of lift coefficient and was equal to:

$$\text{Correction} = -0.0001\alpha^2 + 0.001\alpha + 0.0003 \qquad (22)$$

The hose correction applied equally to all three trailing edges since it was strictly a function of the angle of attack. Table 5 shows the contribution of the lift coefficient hose correction for several angles of attack. As shown in Table 5, the lift coefficient correction was less than 1% over a wide range of angles of attack. The positive corrections are added and the negative corrections

are subtracted. The presence of the hose had a small and correctable effect on the lift coefficient measurements.

Table 5. Summary of Hose Bend Corrections to the Lift Coefficient

Alpha (deg)	Percentage of Final Value
0.69	0.15
2.83	0.32
5.09	0.34
7.18	0.25
9.46	0.08
11.66	-0.14
13.84	-0.41
16.02	-0.73
18.08	-1.09

The lift coefficient was also corrected for the contribution from the thrust of the jet of blowing air. For each wing configuration, an alpha sweep was completed with the blowing air on, but the wind tunnel off. These data files recorded the lift coefficient due to the jet of air alone. Later the wing was tested at the same level of blowing momentum coefficient but with the wind tunnel running. To correct the lift coefficient for the contribution by the jet thrust, the lift coefficient for the jet alone was subtracted from the lift coefficient with the tunnel running. This was done for all data points with blowing.

The jet thrust correction was larger than the hose correction and a function of both the trailing edge shape and the blowing coefficient. Table 6 summarizes the jet thrust corrections which were subtracted from the measured lift coefficient.

Table 6. Summary of Jet Thrust Corrections to the Lift Coefficient

Wing Configuration	Magnitude of Correction	Percent of Final Value
180 deg TE, Low Blowing	0.0055	-0.44
180 deg TE, Medium Blowing	0.0261	-1.43
180 deg TE, High Blowing	0.0381	-1.81
90 deg TE, Low Blowing	0.0310	-2.31
90 deg TE, Medium Blowing	0.0625	-3.75
90 deg TE, High Blowing	0.118	-5.84
45 deg TE, Low Blowing	0.0319	-2.76
45 deg TE, Medium Blowing	0.0611	-5.38
45 deg TE, High Blowing	0.0715	-5.62

As shown in Table 6 above, at a given level of blowing the jet thrust correction percent wise was smallest with the 180 deg trailing edge and largest with the 45 deg trailing edge. Also, increasing the amount of blowing increased the required correction. These trends are caused by two reasons. The magnitude of the correction was smaller for the 180 deg trailing edge than the other two. Also, while the magnitude of the correction was similar for the 90 and 45 deg trailing edges, the 45 deg trailing edge had lower lift coefficients leading to a larger correction as a percent. Overall, the jet thrust correction was much larger than the angle of attack correction. The total correction is the sum of the values in Tables 5 and 6.

Drag Coefficient Corrections

The drag coefficient also was corrected for the blowing air hoses. As for the lift coefficient, the drag coefficient was plotted against the angle of attack for the wing with and without hoses attached, Figure 12.
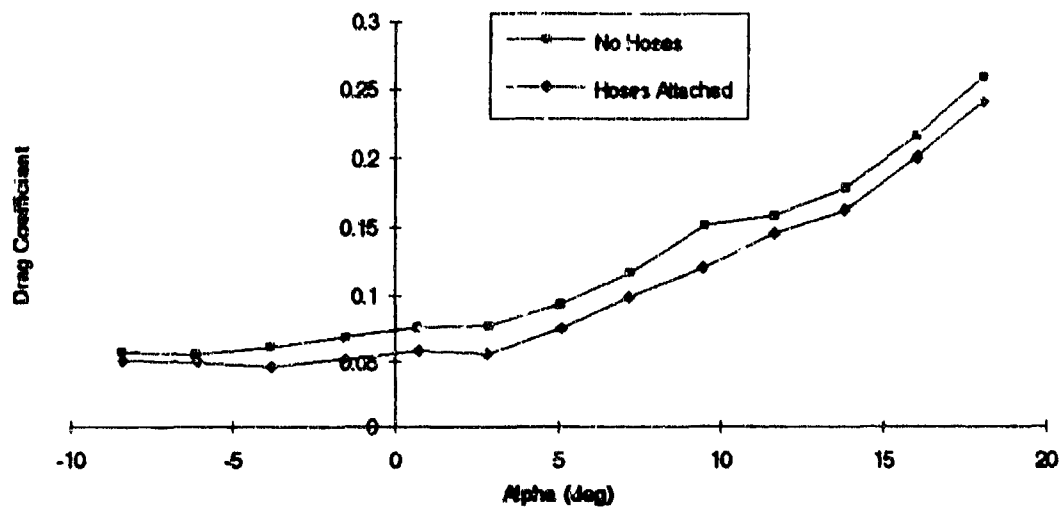
Figure 12. Effect of Blowing Hoses on Drag Coefficient

As shown in the figure above, the hoses reduced the measured drag coefficient. Compared to the lift coefficient case where the lift loads tended to bend the hoses, the drag loads were trying to compress the hose axially. The hose was much stiffer in compression than bending, leading to higher hose bend corrections for the drag coefficient. To obtain the correction, both curves in figure 8 were fitted with second degree polynomials. The correction to be added was the difference between the clean wing and hoses attached configurations. Each drag coefficient point was corrected in this fashion. The correction added to each drag coefficient measurement was a function of the angle of attack and equal to:

$$\text{Correction} = -\ 0.0001\alpha^2 + 0.0008\alpha + 0.017 \qquad (23)$$

This hose correction also applied equally to all three trailing edges since it was strictly a function of the angle of attack. Table 7 shows the contribution of the drag coefficient hose correction for several angles of attack. The positive corrections are added and the negative corrections are subtracted. Although the presence of the hoses had a much larger effect on the drag coefficient than on the lift coefficient it was still correctable.

Table 7. Summary of Hose Bend Corrections to the Drag Coefficient

Alpha (deg)	Percentage of Final Value
0.69	22.7
2.83	24.4
5.09	19.5
7.18	15.1
9.46	11.4
11.66	8.0
13.84	5.2
16.02	2.0
18.08	-0.5

Pulsed Blowing Reductions

Data from the pulsed tests were reduced the same way as the steady state blowing tests. It should be noted that because the data acquisition system takes many measurements and averages them while at a single data point, transient forces and moments are averaged out in the output.

VI. RESULTS

Hysteresis Check

The results of the hysteresis test are in Figure 13. At the higher angles of attack there is little indication of hysteresis. However, at angles of attack less than zero the lift measured while alpha was increasing was higher than that measured with alpha decreasing. The difference between the two curves is small, on the order of 0.046, but quite large when expressed as a percent of lift coefficient because the lift coefficient is very small at those angles of attack. The magnitude of the hysteresis at negative angles of attack is similar to that of the jet thrust correction and larger than the hose bend correction to the lift coefficient.
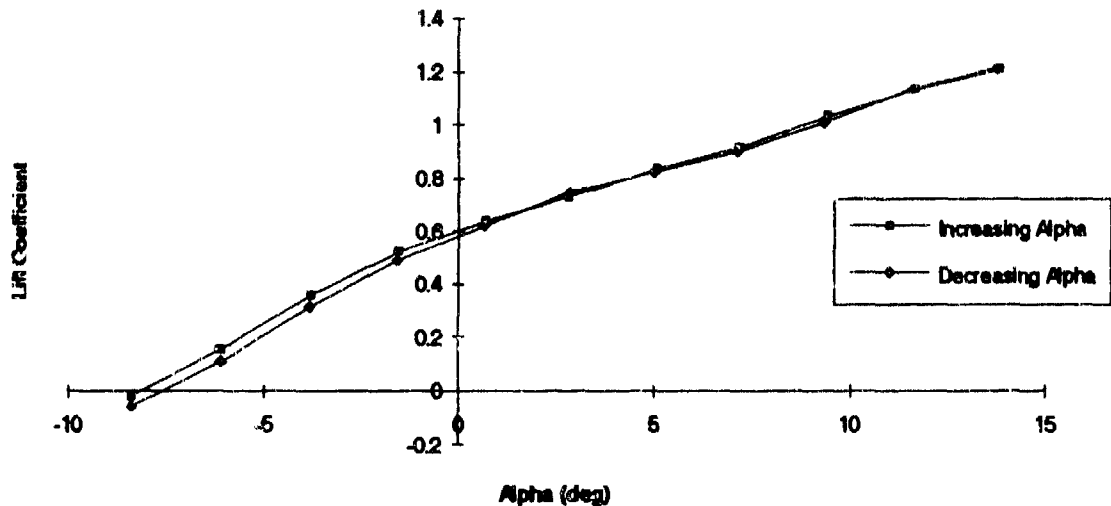
Figure 13. Hysteresis Results, 180 deg Trailing Edge

Repeatability Check

Test repeatability was checked by repeating points of an earlier run later in the test. The results, shown in Figure 14, suggest a high degree of repeatability. The maximum difference in lift coefficient between the two tests, for the same angle of attack was 0.015. At the higher angles of attack, this corresponded to an error of 3.3%.

Figure 14. Repeatability Check, 45 deg Trailing Edge

180 degree Trailing Edge

First, lift data for the 180 deg trailing edge will be presented. The lift coefficient was plotted against momentum coefficient for four angles of attack, Figure 15.

Figure 15. Effect of Blowing on Lift Coefficient, 180 deg Trailing Edge

From Figure 15, increasing the blowing at a given fixed angle of attack increases the lift coefficient as expected. The effect of changing the angle of attack only shifts the C_L vs. C_μ curve up or down. Also, along a given angle of attack curve, th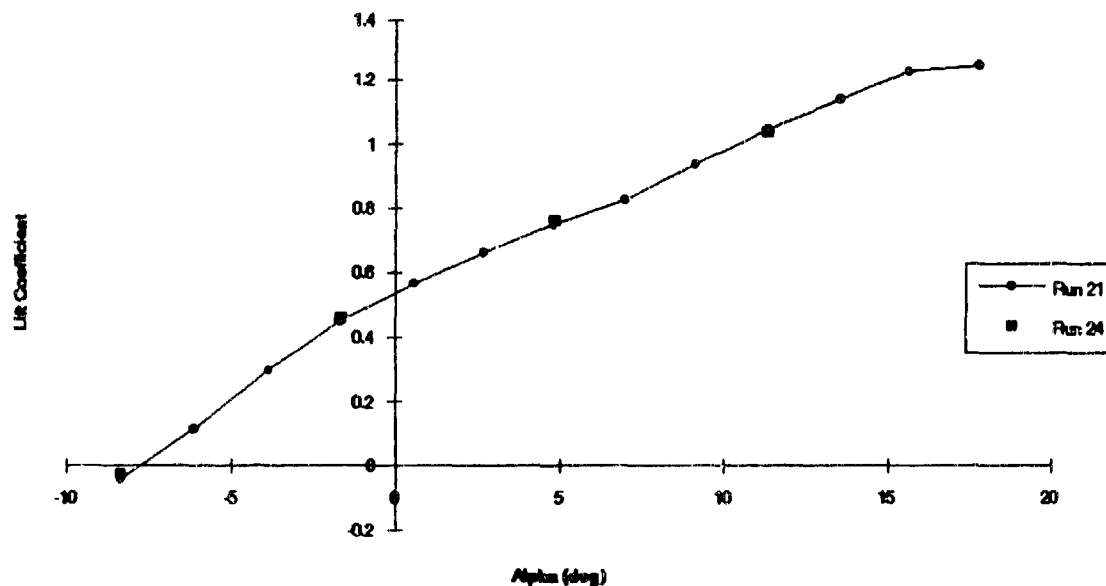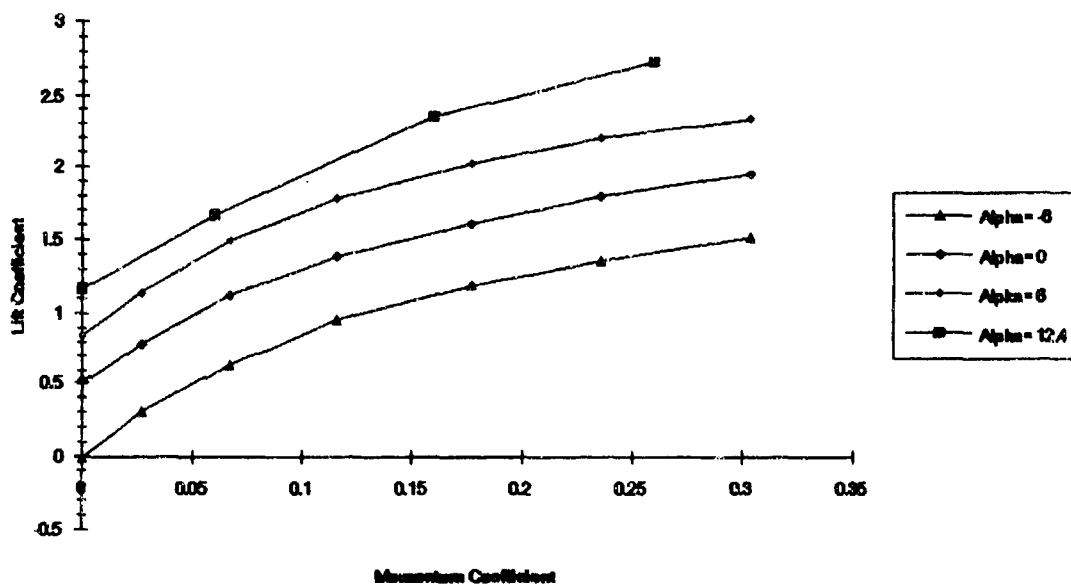e slope of the curve decreases as the momentum coefficient is increased. This suggests that a limit on how high the lift coefficient can be raised with increasing blowing is being approached.

Generally, the curves of constant angle of attack in Figure 15 are uniformly spaced. The exception is the curve at an angle of attack of 12.4 degrees. That particular curve was assembled from data from four different runs where the blowing coefficient was held constant and the angle of attack was varied. The data point at $C\mu$=0.06 was approaching stall at this angle of attack and blowing combination and consequently has a little lower value of lift coefficient. The other three data points on this curve were not near the stall angle of attack.

Figure 16 shows the lift to measured drag ratio plotted against the momentum coefficient. As the momentum coefficient is increases at a given angle of attack the L/D ratio rises to a maximum before decreasing and finally leveling off. The same trend occurs for all three angles of attack shown but each has a unique level of blowing coefficient where L/D is a maximum. The

29

peak lift to drag ratio occurs at relatively low values of momentum coefficient for all three angles. For momentum coefficients greater than 0.25, all the L/D ratio curves level out. This trend indicates a practical limit to blowing and is true for all three angles of attack examined. The trends in the figure suggest that a sufficiently high angle of attack, the peak lift to drag ratio will occur at zero blowing.
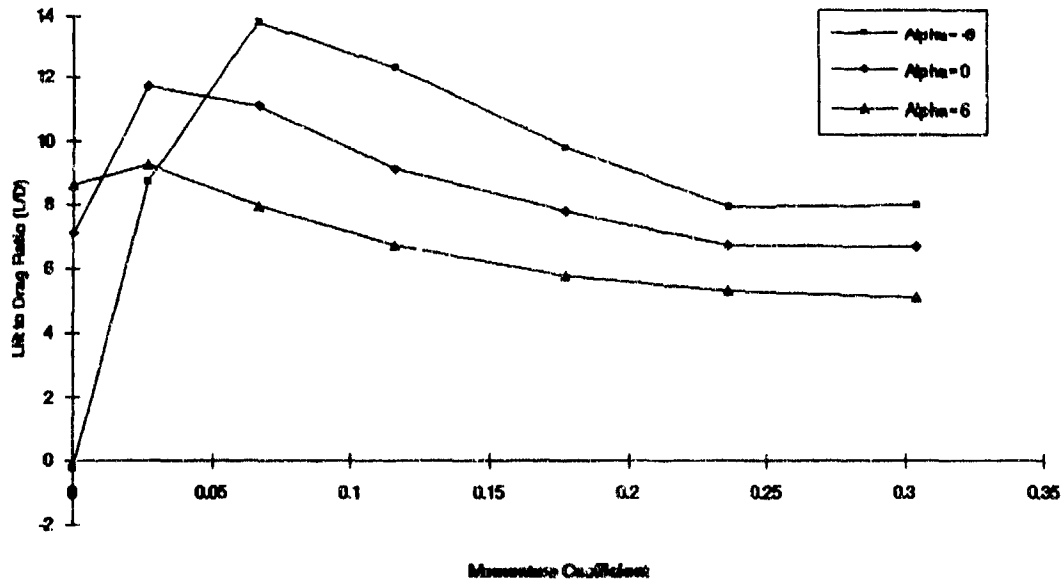
Figure 16. Effect of Blowing on Lift to Drag Ratio, 180 deg Trailing Edge

The pitching moment about the model center of gravity is plotted against the blowing coefficient at three angles of attack for the 180 deg trailing edge in Figure 17. Along a given angle of attack the pitching moment decreases as the blowing is increased. This corresponds to an increasing nose down moment as the blowing is raised. Increasing the angle of attack reduced the nose down moment.

30
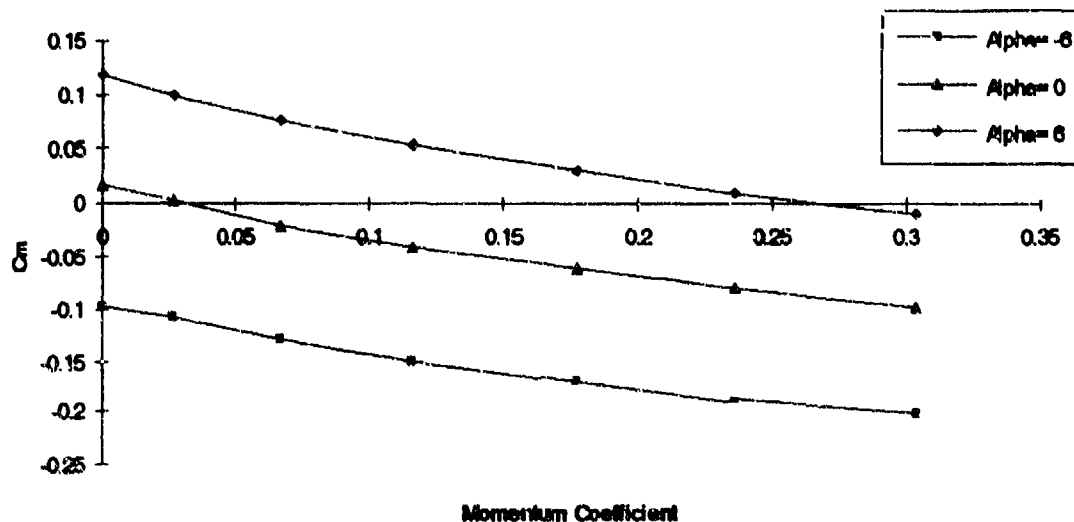
Figure 17. Effect of Blowing on Pitching Moment, 180 deg Trailing Edge

Comparison of Trailing Edge Shapes

First the force and moment data will be discussed, followed by the pressure data. One of the objectives of this research investigation was to determine if partially rounded trailing edges could have equal or better performance than a full 180 deg rounded trailing edge. The lift coefficient for the three trailing edges is compared at maximum blowing in Figure 18. The performance of the 180 and 90 deg trailing edges is nearly equal because the 90 deg case has only 4% less lift than the 180 deg trailing edge with 7% less blowing at the same angle of attack, zero. The 45 deg trailing edge has 40% less lift than the 180 deg trailing edge.
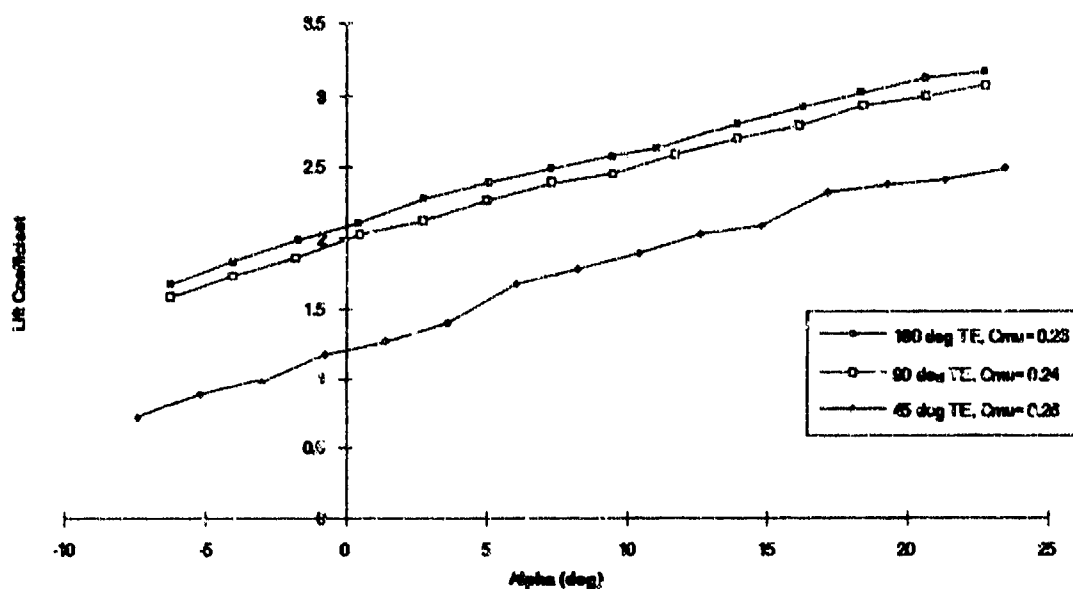
Figure 18. Effect of Blowing on Lift Coefficient for Three Trailing Edges

The effect of increased blowing on each trailing edge is considered next. Figures 19 through 21 show the lift coefficient plotted against the angle of attack.
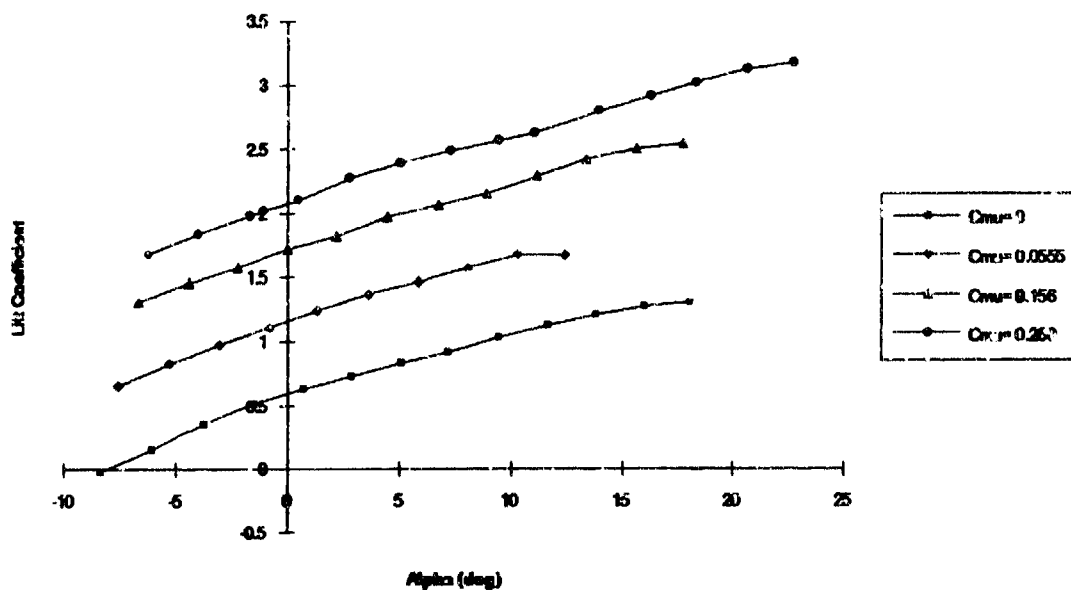
Figure 19. Effect of Blowing, 180 deg, Trailing Edge
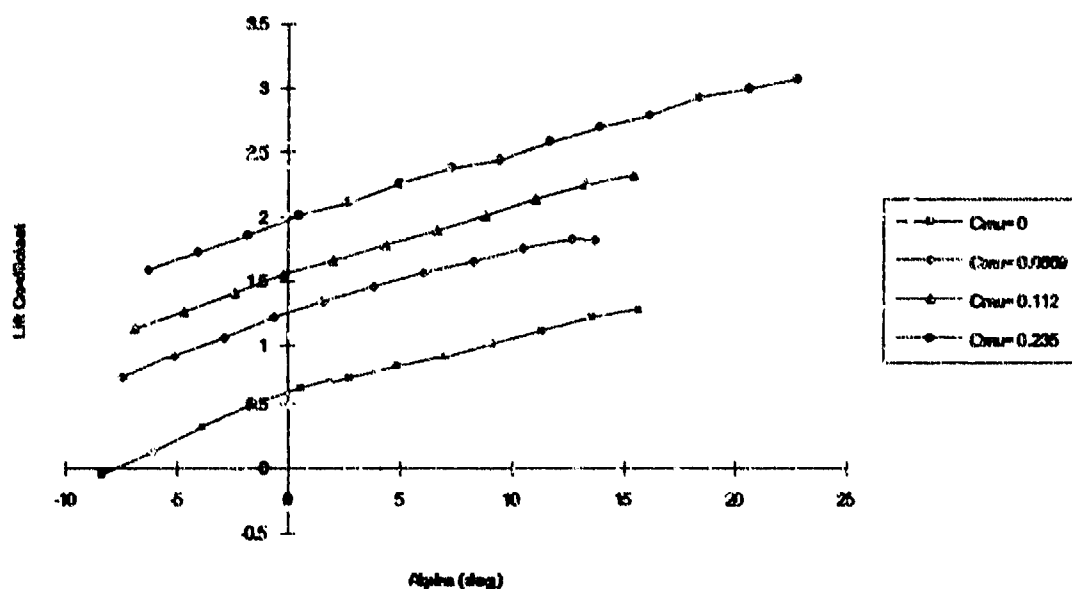
Figure 20. Effect of Blowing, 90 deg Trailing Edge

Figures 19 and 20 have similar characteristics. Increasing the blowing shifts the C_L vs. alpha curve up. Also, C_L vs. alpha curves remain straight and parallel with no change in slope. Increasing the blowing also shifts the stall angle of attack. For the 180 deg trailing edge case with no blowing, the wing stalls at about 18 deg. When blowing is first started, the angle of stall decreases to 13 deg. As the amount of blowing is increased, the angle of stall increases. At maximum blowing, the stall angle is approximately 22 deg. Low blowing rates disrupt the flow of air at the trailing edge and lead to early separation, but at higher blowing rates, the air over the upper surface is energized and remains attached to the wing at higher angles of attack. This trend is also true for the 90 deg and 45 deg trailing edges, Figures 20 and 21.
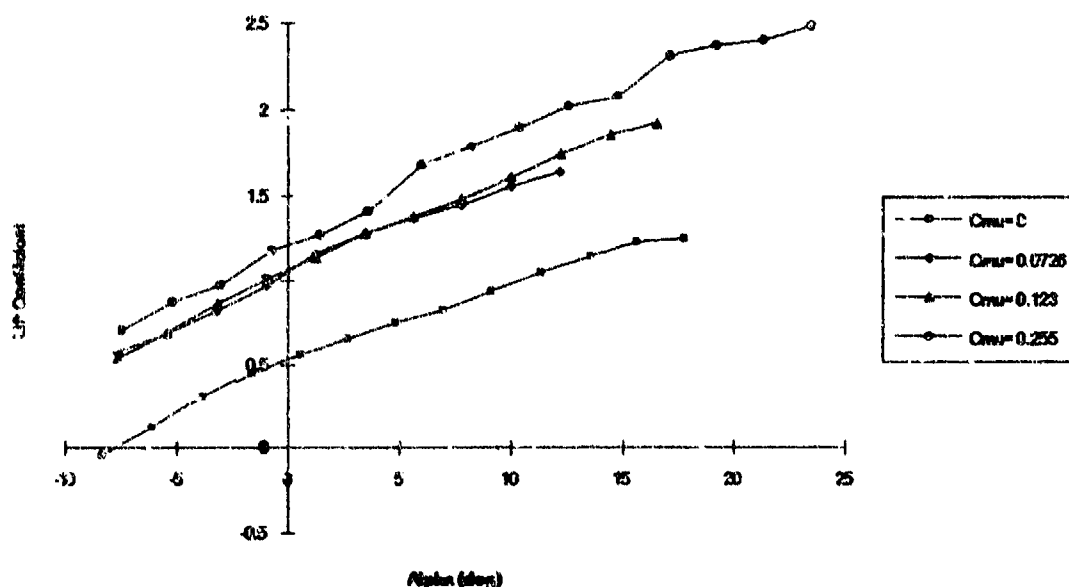
Figure 21. Effect of Blowing, 45 deg Trailing Edge

For the 45 deg trailing edge, Figure 21, the results are mixed. Increasing blowing does not raise the lift coefficient in all cases. For example, there is little difference in lift coefficient between C_μ=0.0726 and C_μ=0.123. The higher blowing only allowed higher angles of attack and produced an erratic lift coefficient curve.

The lift coefficient at maximum blowing and alpha equal to nearly 20 deg was compared for all three trailing edges. The 180 deg trailing edge had a lift coefficient of 3.12. At similar conditions, the 90 deg trailing edge had a lift coefficient of 2.99, only 4.2% less than the 180 deg trailing edge. Also at similar conditions, the 45 deg trailing edge had a lift coefficient of 2.36, 24% less than the 180 deg trailing edge.

As shown by Equations 5 and 6 there is a limit to the maximum lift coefficient of a circulation control wing. For the 180 deg trailing edge with an aspect ratio of 3.99, the two limits for the lift coefficient are 3.41 and 4.83. From Figure 19, the maximum lift coefficient measured during testing was 3.17, lower than either of the two limits. This points out that though the lift may be leveling off with increasing blowing, as shown in Figure 15, there is still more lift to be gained by increasing the amount of blowing.

34

The equivalent drag of the three trailing edges at maximum blowing is compared in Figure 22. The 180 deg trailing edge had the highest drag of the three configurations. At an angle of attack of approximately zero the 90 deg trailing edge had 15% less drag and the 45 deg trailing edge had 34% less drag.
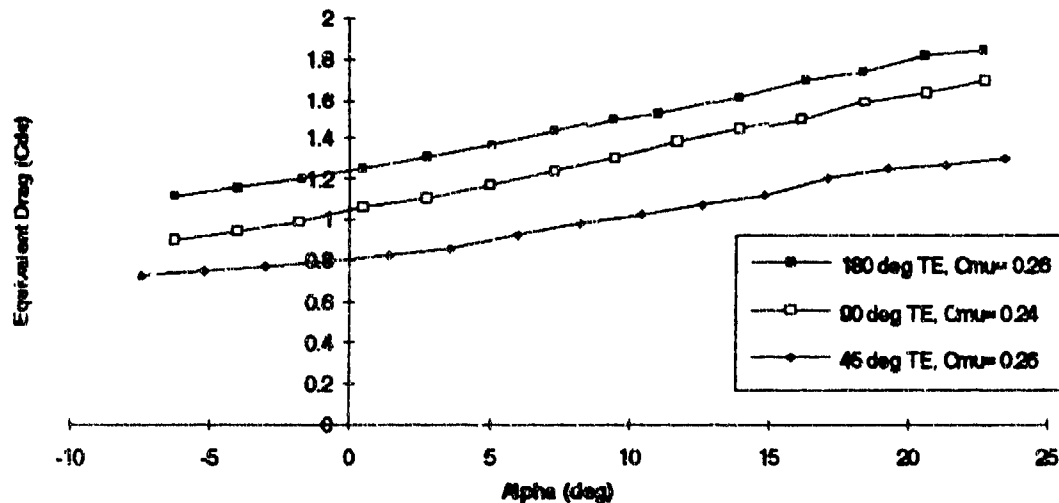
Figure 22. Comparison of Lift Performance, Maximum Blowing

The equivalent drag for each of the three trailing edges is shown in Figures 23 through 25. For the 180 deg trailing edge, Figure 23, the increase in drag is equal to the equivalent drag contribution. At the higher blowing rates the drag is very substantial. The same trends are noted for the other two trailing edges, Figures 24 and 25.
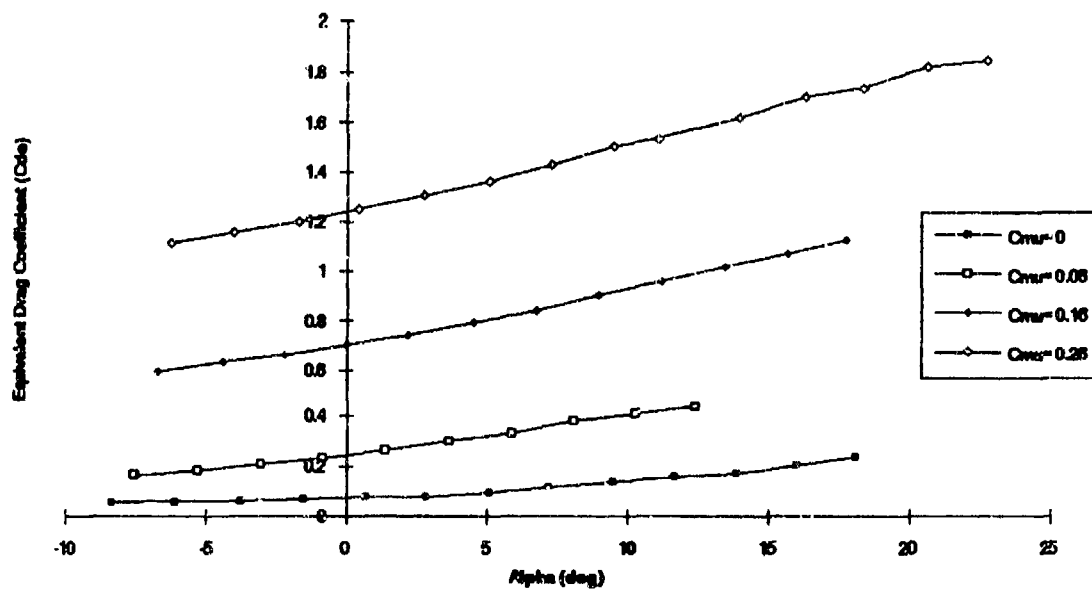
Figure 23. Equivalent Drag, 180 deg Trailing Edge
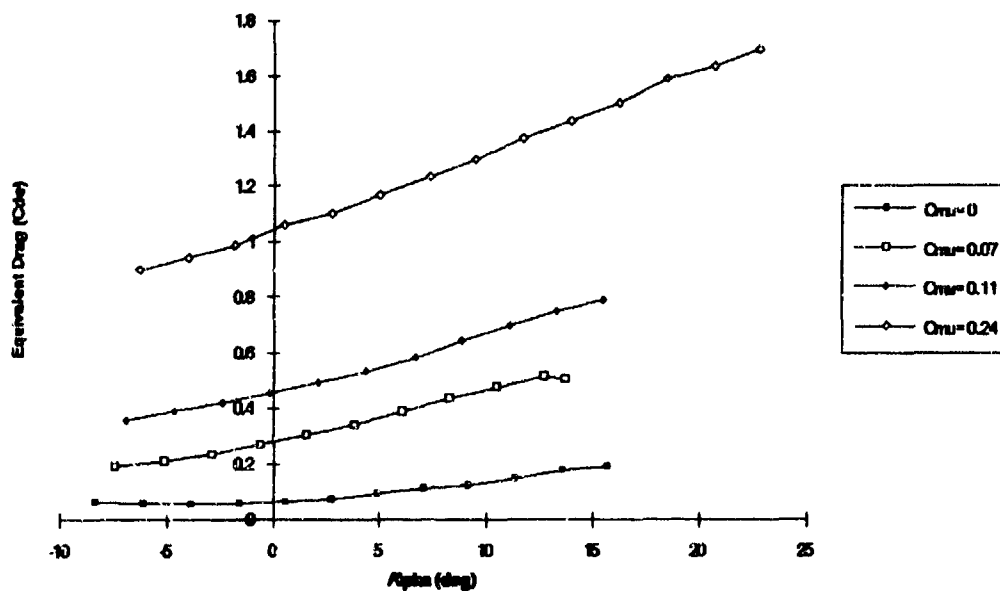
Figure 24. Equivalent Drag, 90 deg Trailing Edge
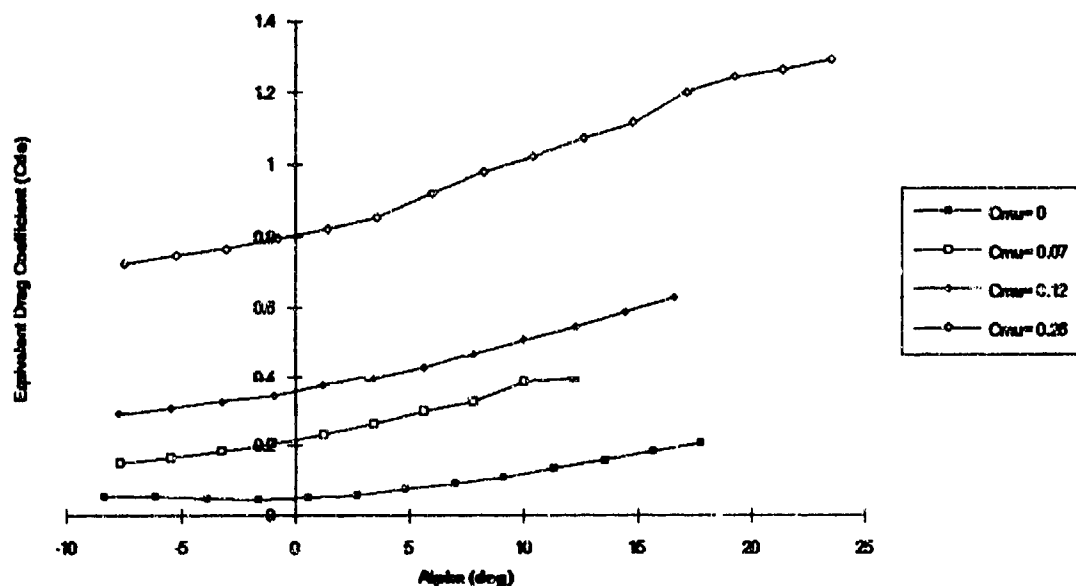
Figure 25. Equivalent Drag, 45 deg Trailing Edge

The pitching moments about the wing center of gravity for the three trailing edges is compared at maximum blowing, Figure 26. The 180 deg and 90 deg trailing edges have nearly identical curves. The 45 deg trailing edge has a much different curve with the pitching moment being positive over most of the range of alpha.
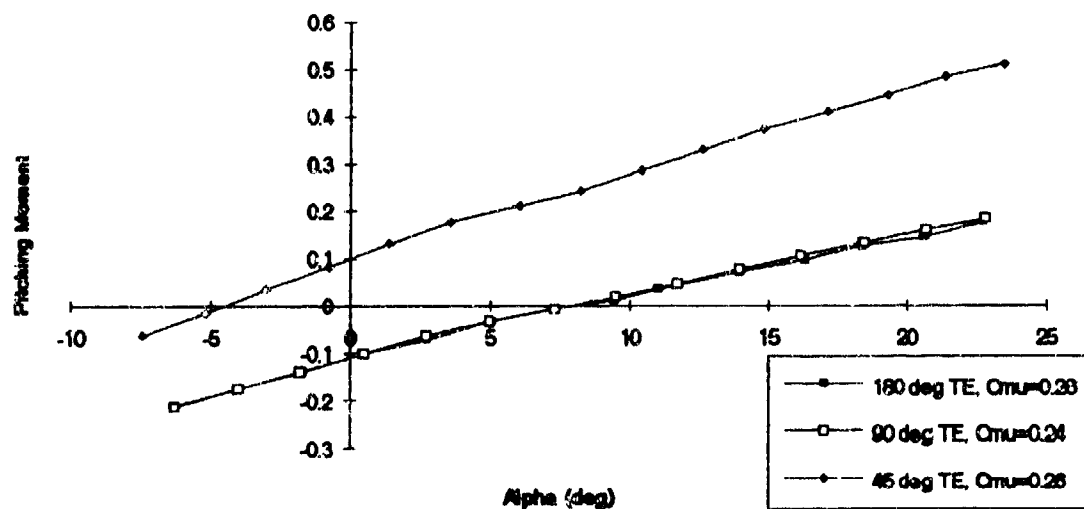
Figure 26. Effect of Blowing on Pitching Moment for Three Trailing Edges

37

The pitching moment curves for the individual trailing edges at several levels of blowing follow in Figures 27 through 29. The set of curves for the 180 and 90 deg trailing edges, Figures 27 and 28, are very similar. The pitching moment curve for the 45 deg trailing edge, Figure 29, is different because all of the Cm vs. Alpha curves for the different levels of blowing lie on one line. For the 45 deg trailing edge the pitching moment is independent of the amount of blowing and only a function of the angle of attack.
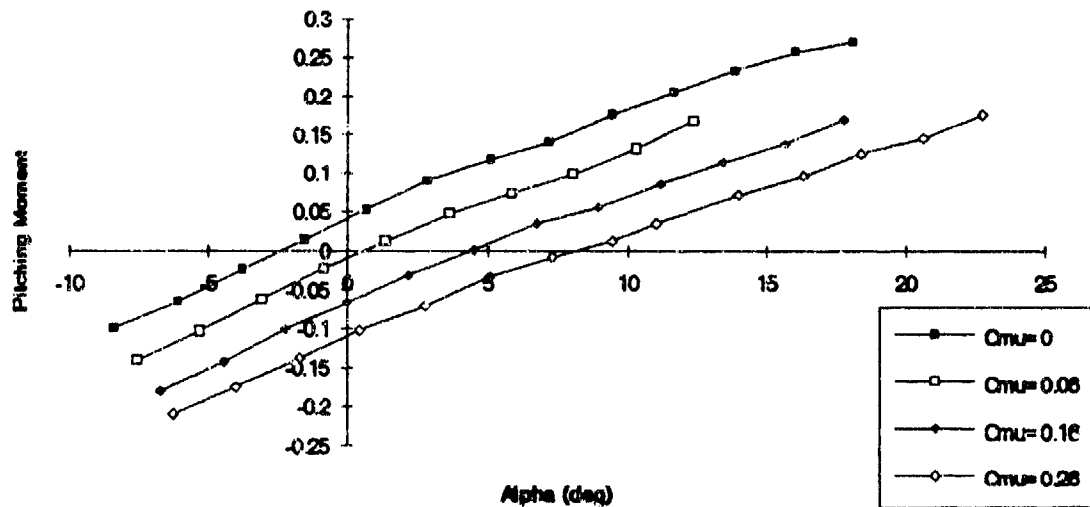
Figure 27. Pitching Moment, 180 deg Trailing Edge
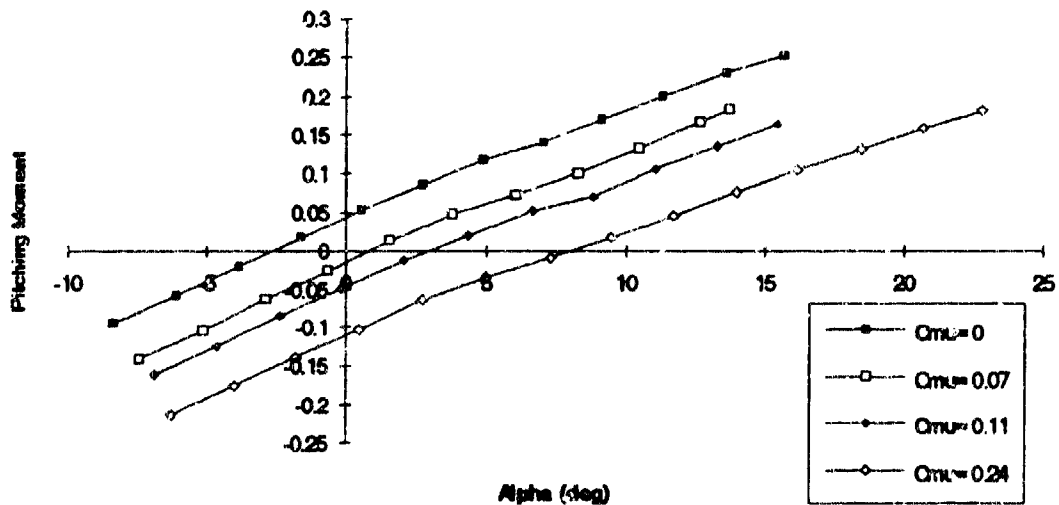
Figure 28. Pitching Moment, 90 deg Trailing Edge
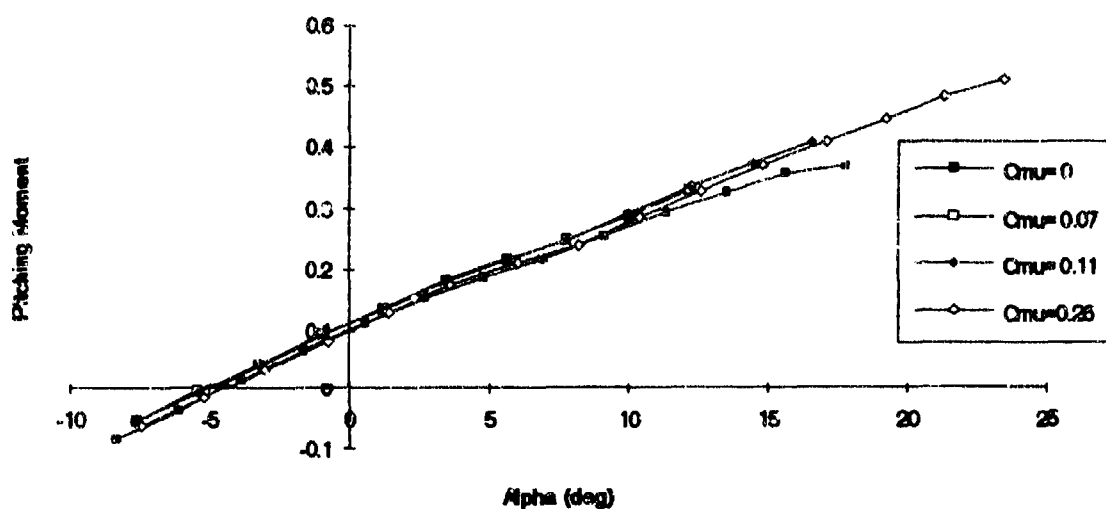
Figure 29. Pitching Moment, 45 deg Trailing Edge

Pressure coefficient plots are considered next. First, the 180 deg trailing edge is shown, Figure 30, with no blowing. It is followed by three plots, Figures 31 through 33 of the three trailing edges at maximum blowing. All plots are at an angle of attack of approximately zero.
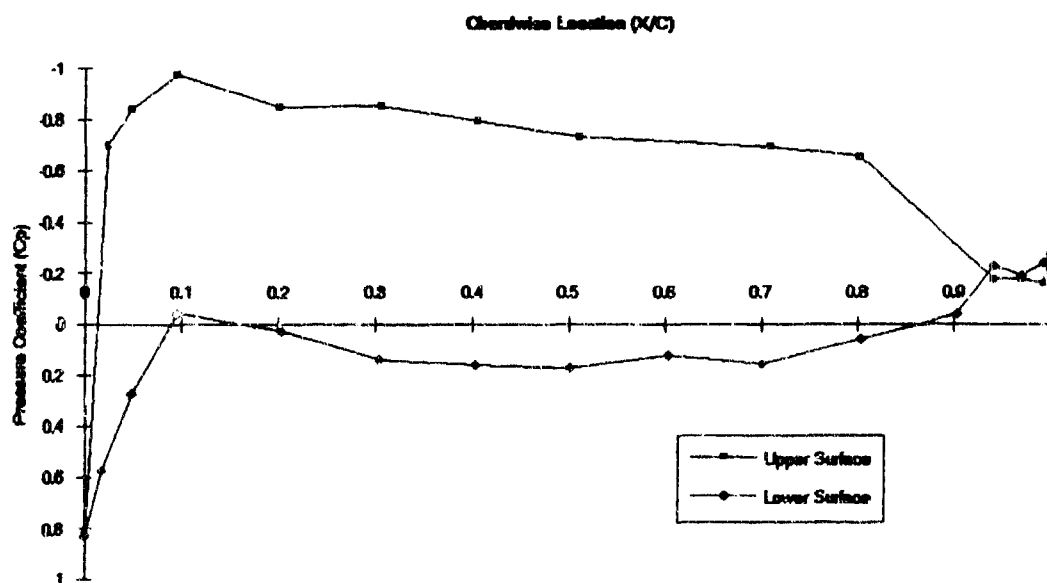
Figure 30. Pressure Coefficient, 180 deg Trailing Edge, $C_\mu=0$, alpha=0.69
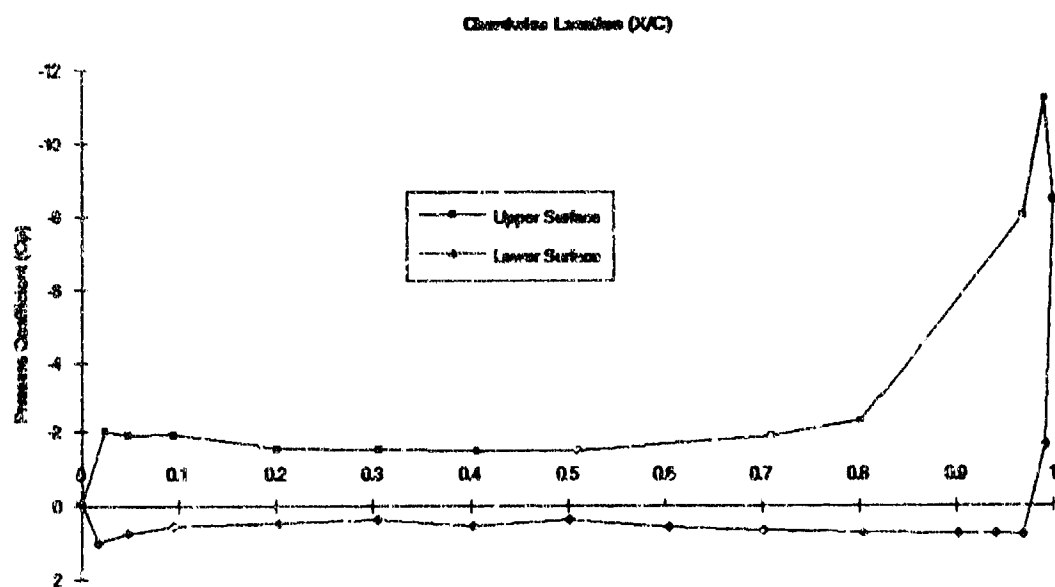
Figure 31. Pressure Coefficient, 180 deg Trailing Edge, C_μ=0.26, alpha=0.44
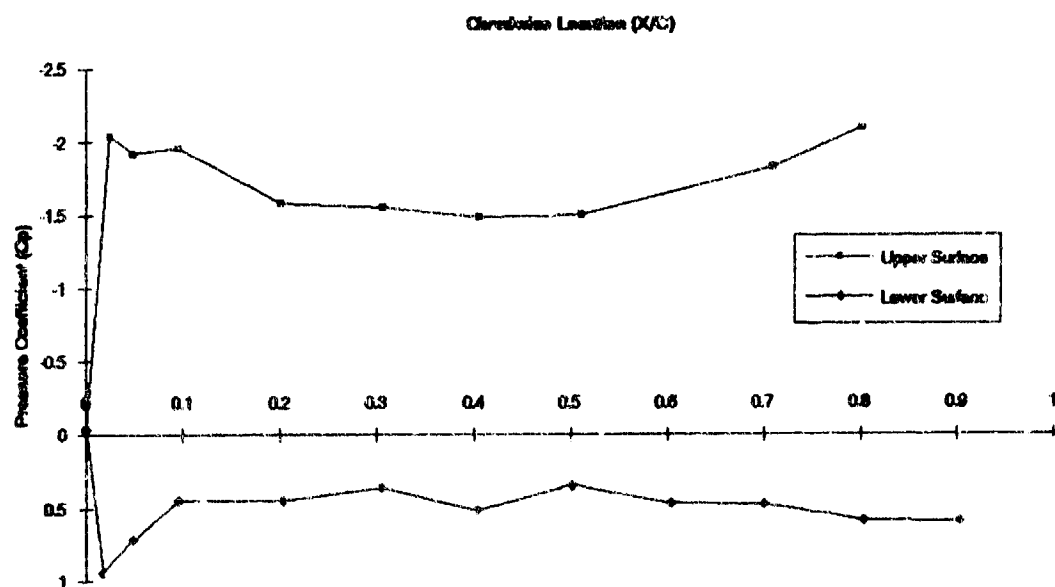
Figure 32. Pressure Coefficient, 90 deg Trailing Edge, C_μ=0.24, alpha=0.48
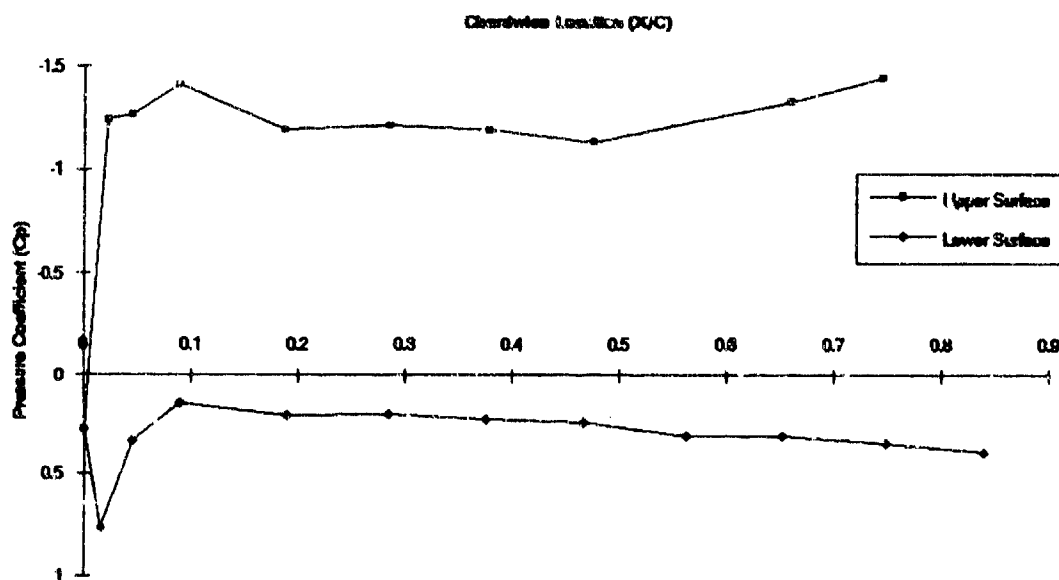
Figure 33. Pressure Coefficient, 45 deg Trailing Edge, C_μ=0.26, alpha=0.75

Figure 30 shows the pressure coefficient plot of the wing with the 180 deg trailing edge and no blowing. The stagnation point lies on the leading edge and there is a mild low pressure region at the trailing edge. The pressure coefficient was plotted for the 180 deg trailing edge at maximum blowing, Figure 31. The increased circulation induced by the blowing has moved the front stagnation point from the leading edge back to the x/c=0.17 location on the lower surface. Most significantly, there is a very strong low pressure region at the rear of the wing. This suction peak at maximum blowing causes an increase in the drag coefficient compared to the unblown wing. Figure 32 shows the wing at a similar angle of attack and blowing coefficient but with the 90 deg trailing edge. The pressure coefficient data is incomplete because the trailing edge was not instrumented for this and the 45 degree case. Again, increased circulation moved the leading edge stagnation point moved rearward to the lower surface. As the rear of the wing is approached, the pressure coefficient becomes increasingly negative, suggesting a low pressure region at the trailing edge like the first configuration. When examining Figure 33, the 45 deg trailing edge case, the

pressure coefficient is less across the upper surface than the other two configurations, leading to a decreased lift coefficient. The four configurations are compared in Table 8.

Table 8. Lift and Drag Data for Various Configurations

T. E.	Alpha	C_μ	C_L	C_{De}	L/De
180	0.69	0.0	0.64	0.077	8.27
180	0.44	0.26	2.14	1.25	1.71
90	0.48	0.24	2.14	1.06	2.02
45	-0.75	0.26	1.25	0.795	1.57

When comparing the blown 180 deg and 90 deg trailing edges, the lift is equal, but the lift for the 45 deg trailing edge is 42% less. The equivalent drag for the 90 deg trailing edge is 15% less than that for the 180 deg trailing edge. This suggests that though the 90 deg trailing edge also may have a suction peak, it is probably less than the 180 deg trailing edge. The 45 deg trailing edge has lower lift and drag coefficients than the first two configurations. A final comparison is made using the lift to equivalent drag ratio. This ratio shows that increasing the circulation about the wing raises the drag more than the lift since all blown L/De are less than the unblown cases. Of the blown wings, the 90 deg trailing edge configuration has the best lift to drag ratio, entirely because of the lower drag compared to the 180 deg configuration.

Pulsed Testing

First, the shape of the pressure pulse will be discussed, followed by force and moment results. The shape of the pressure pulse was very distinct as it left the pulser valve and merged with the bypassed air. A typical single pulse at this location is given in Figure 34. The mean pressure was 22.3 psig and the amplitude was 2.0 psi
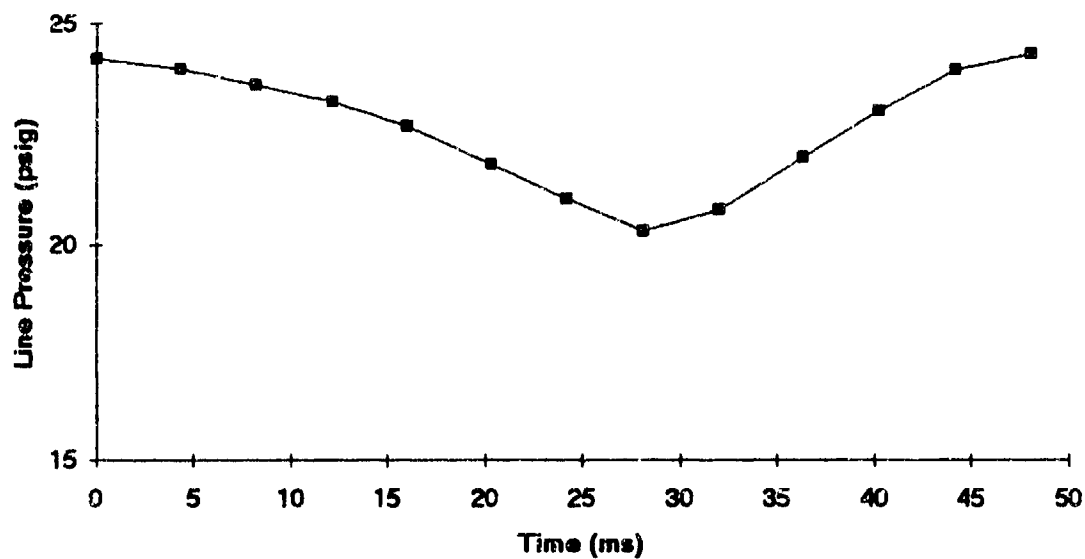
Figure 34. Pressure Pulse Near Pulser Valve, Low Blowing, 20.8 Hz

As the air traveled down the 1/2 inch supply line to the model, the mean and amplitude pressures dropped and the wave form became distorted. Figures 35 through 38 give a typical pressure pulse as measured at the entrance to the model after passing through approximately 12 feet of hose. The effect of increasing blowing on the shape of the pulse is shown progressively in Figures 35 through 37.
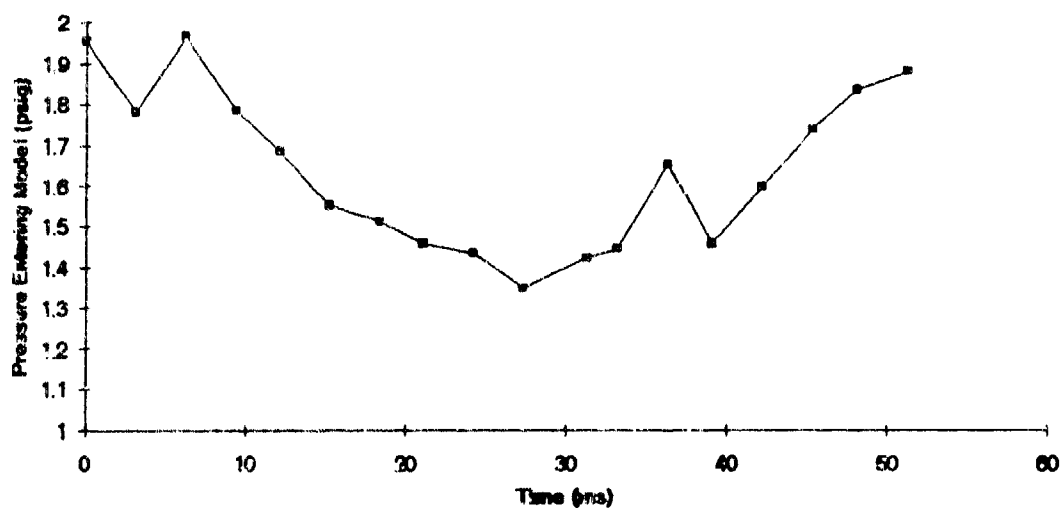
Figure 35. Pressure Pulse At Model, Low Blowing, 19.9 Hz
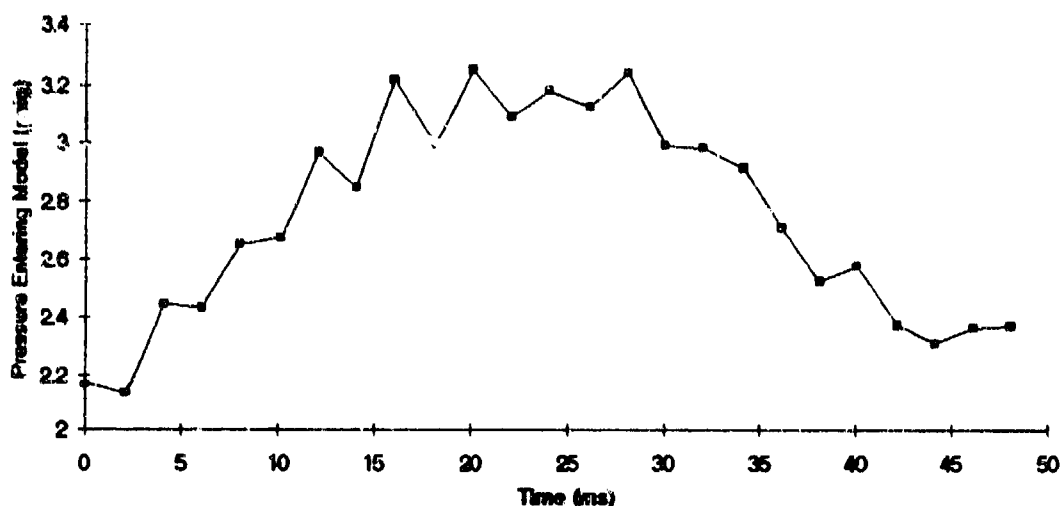
Figure 36. Pressure Pulse At Model, Medium Blowing, 20.4 Hz
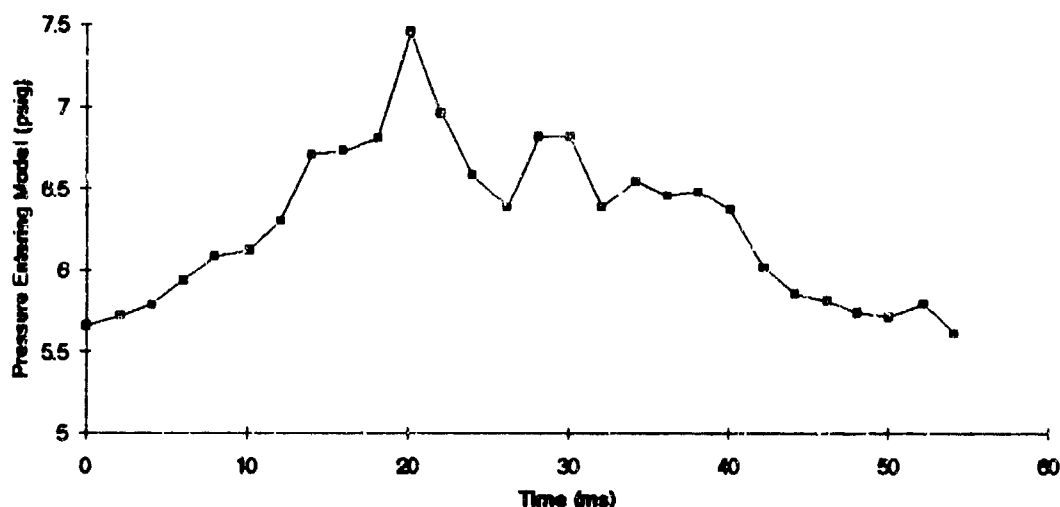
Figure 37. Pressure Pulse At Model, High Blowing, 19.8 Hz

The pressure drop through the hoses was quite large and altered the pressure pulse entering the model. For example, at low blowing the mean pressure measured at the model was 1.7 psig compared to 22.3 psig at the pulser valve and the amplitude was reduced from 2.0 psi to 0.3 psi. As the blowing increased, the pressure pulse shape has more and more noise in it, so that at maximum blowing, Figure 37, there is no well defined pulse entering the model.

In Figure 38 the pressure pulse shape at the model is shown at a higher pulsing frequency, 40.2 Hz. The effect of raising the frequency while keeping the blowing constant can be seen by comparing Figure 36 and Figure 38, both at medium blowing. Raising the pulsing frequency also leads to a distorted waveform.
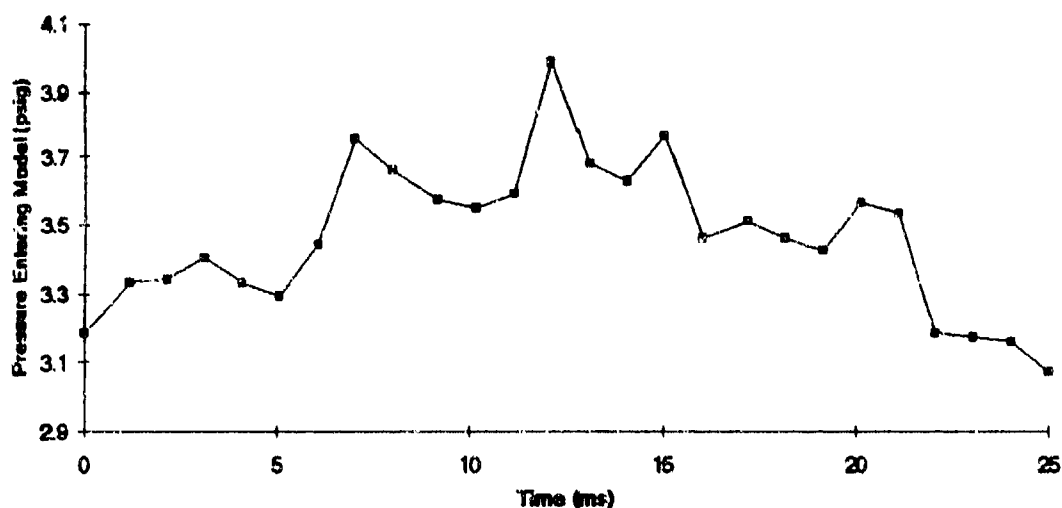
Figure 38. Pressure Pulse At Model, Medium Blowing, 40.2 Hz

The effect of pulsing on the lift coefficient is examined next. The lift coefficient for the 180 deg trailing edge is plotted for three angles of attack at various pulsing frequencies, Figures 39 through 41. At low blowing levels, Figure 39, the lift coefficient decreases as the pulsing frequency increases for two angles of attack, -1.1 deg and 3.3 deg. The pulsing increased the lift coefficient for an angle of attack of 1.0 deg.

45
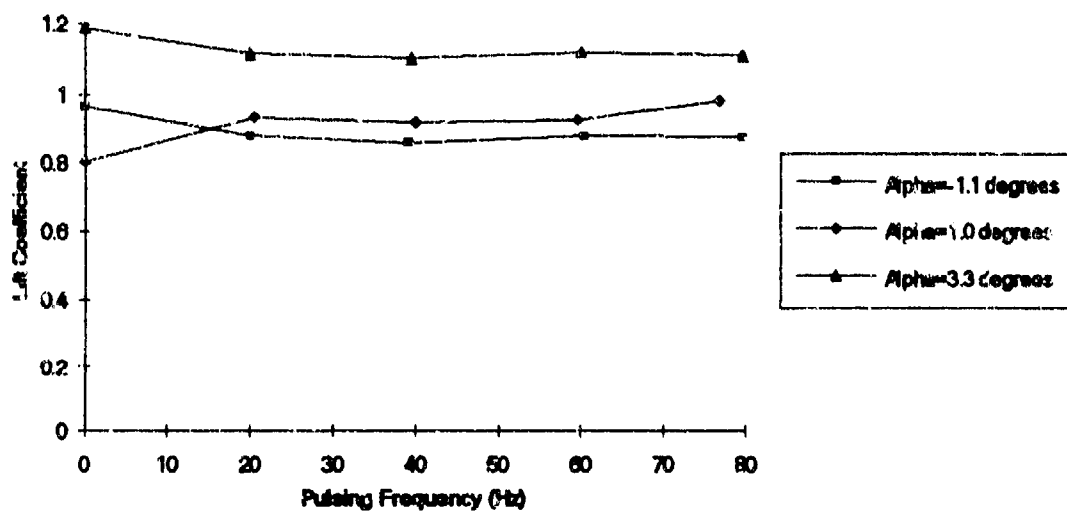
Figure 39. Effect of Pulsing Frequency on Lift, C_μ=0.018

Mixed results also occur at a medium level of blowing, Figure 40. At this level of blowing the lift coefficient increases at the two higher angles of attack as the pulsing frequency was raised from steady blowing to 20 Hz. Pulsing decreased the lift at an angle of attack of -0.9 deg. Results for all three angles of attack remain steady as the frequency is increased above 20 Hz. This is caused by the break-down of the pressure pulses when the frequency is increased shown earlier. Increasing the frequency beyond 20 Hz only results in random pressure fluctuations reaching the model instead of distinct pulses.
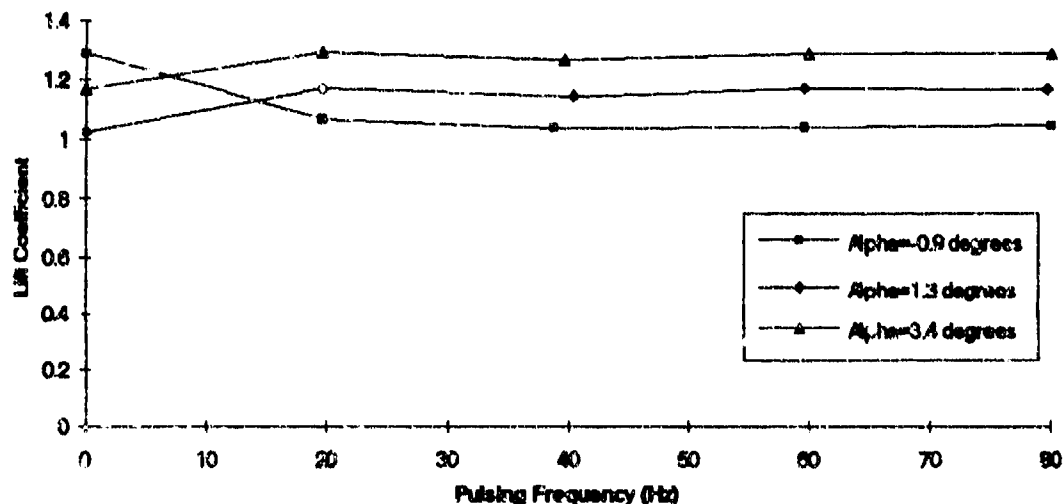
Figure 40. Effect of Pulsing Frequency on Lift, C_μ=0.089

At the highest level of pulsed blowing, Figure 41, the lift essentially remains unchanged as the pulsing frequency is raised. This is due to the severely distorted pressure pulse at high blowing reaching the model noted earlier. The model was not receiving distinct pressure pulses.
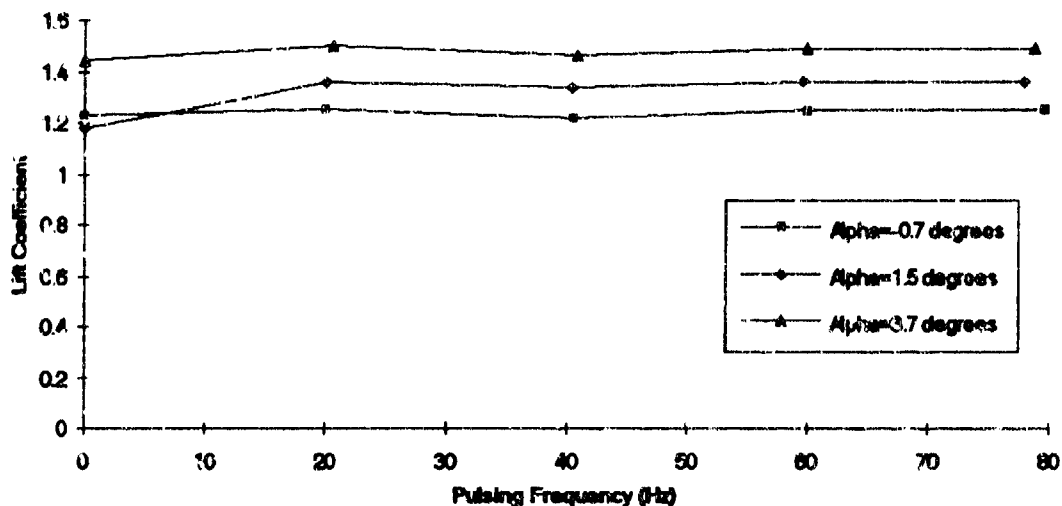
Figure 41. Effect of Pulsing Frequency on Lift, C_μ=0.11

Overall, the lift coefficient results of pulsing the blowing air to the model are mixed. The lack of a clear trend as the frequency or blowing is increased is because the pressure pulse reaching the model is not a clear sinusoidal signal, but something approaching noise.

VII. CONCLUSIONS

1. The maximum lift possible from this wing was not reached and higher lift coefficients can be achieved with higher blowing rates. Test data shows the rate of increase of lift with higher blowing is decreasing, indicating that a limit to the lift coefficient is being approached. The exception is the 45 deg trailing edge, where increasing the blowing gave mixed results.

2. The 90 deg trailing edge shows promise as a better trailing edge for a circulation control wing. The lift performance of the wing with this trailing edge was essentially equal to that of the 180 deg trailing edge. The equivalent drag of the wing with the 90 deg trailing edge was as much as 15% less than the wing with the 180 degree trailing edge. Pitching moment characteristics for the 180 and 90 deg trailing edges were basically the same.

3. The 45 deg trailing edge had lift, drag, and pitching moment characteristics much different than the 180 deg and 90 deg trailing edges. The lift on the wing with the 45 deg trailing edge was less than that with the other two trailing edges and as much as 40% less than the 180 deg trailing edge at zero degrees angle of attack. The equivalent drag of the wing with the 45 deg trailing edge was as much as 35% less than the 180 deg trailing edge. The pitching moment was independent of the amount of blowing with this trailing edge.

4. Results from the pulsed tests were mixed because the model was not receiving clear distinct pressure pulses. By the time the pressure pulse traveled through the hose and reached the model it was dampened out. This situation was aggravated by higher blowing rates and higher pulsing frequencies.

VIII. RECOMMENDATIONS

1. To obtain a complete pressure coefficient profile around the entire wing, it is recommended that the 90 and 45 degree trailing edges be instrumented to measure pressure. With these measurements, it can be determined if the 90 degree trailing edge has a less powerful suction peak than the 180 degree trailing edge.

2. When the actual pressure pulse entering the model was measured, it was found to be very irregular. Much of the distortion was due to the pressure pulse traveling through the long, small diameter hose from the pulser valve to the model. To obtain more control and achieve a more distinct pressure pulse at the wing, it is recommended that the pulser valve be brought closer to the model by installing it in the tunnel downstream of the test section, or inside of the model.

3. Since the maximum lift coefficient was not reached, it is recommended that the model be tested at still higher levels of blowing to see if the limits proposed by McCormick[9] can be reached.

4. If a new model is to be constructed of similar size, it is recommended that the amount of instrumentation inside of the model (primarily static pressure ports) be limited to what is absolutely necessary. The small volume of the current model presented great difficulty to the model builders and greatly lengthened the time required to build the model.

REFERENCES

1. Englar, R. J., Low-Speed Aerodynamic Characteristics of a Small, Fixed-Trailing-Edge Circulation Control Wing Configuration Fitted to a Supercritical Airfoil. Report Number DTNSRDC/ASED-81/08, David W. Taylor Naval Ship Research and Development Center, Bethesda, Maryland, March 1981.

2. Grumman Aerospace Corporation, Design of an A-6A Flight Demonstrator Aircraft Modified with a Circulation Control Wing (CCW). NSRDC Report CCW/1255-RE-01, Naval Ship Research and Development Center, Bethesda, Maryland, January 1978.

3. Harvell, John K., An Experimental/Analytical Investigation into the Performance of a 20-Percent Thick, 8.5 Percent Cambered Circulation Controlled Airfoil. MS Thesis, AFIT/GAE/AA/82D-13. School of Engineering, Air Force Institute of Technology (AU), Wright-Patterson AFB, OH, December 1982 (AD-124732).

4. Trainor, John W., A Wind Tunnel Study of a Sting-Mounted Circulation Control Wing. MS Thesis, AFIT/GAE/ENY/89D-38. School of Engineering, Air Force Institute of Technology (AU), Wright-Patterson AFB, OH, December 1989.

5. Pelletier, Michael E., An Experimental Study of a Sting-Mounted Single-Slot Circulation Control Wing. MS Thesis, AFIT/GAE/ENY/90D-18. School of Engineering, Air Force Institute of Technology (AU), Wright-Patterson AFB, OH, December 1990.

6. Lacher, Steven J., An Experimental Study of a Sting-Mounted Circulation Control Wing. MS Thesis, AFIT/GAE/ENY/91D-4. School of Engineering, Air Force Institute of Technology (AU), Wright-Patterson AFB, OH, December 1991.

7. Kuethe, A.M. and Chow, C-Y, Foundations of Aerodynamics, John Wiley and Sons. Inc., New York, New York, 1986.

8. Kohlman, D. L., Introduction to V/STOL Airplanes. Iowa State University Press, Ames, Iowa, 1981.

9. McCormick, Barnes W., Aerodynamics of V/STOL Flight. Academic Press, Inc., Orlando, Florida, 1967.

10. Wood, N. and Nielson, J., Circulation Control Airfoils Past, Present, and Future. AIAA Paper 85-0204. American Institute of Aeronautics and Astronautics, January 1985.

11. Rae, William H. and Pope, Alan, Low Speed Wind Tunnel Testing. John Wiley & Sons, New York, New York, 1984.

APPENDIX

Corrected Force Balance Data

cir3_001.### from cir3001.OUT
Circulation Control Run
1:50:29pm on 9/16/92
Description Configuration No Hoses
Comments No Problems
Barometric 29.3450
Re=497000
Cmu=0

Pt	Alp. corr.	WindCl	WindCd	WindCm
1	-8.42	-1.35E-02	5.82E-02	-0.1074
2	-6.14	1.41E-01	5.67E-02	-0.0691
3	-3.92	3.43E-01	6.19E-02	-0.0256
4	-1.53	5.21E-01	6.92E-02	0.0169
5	0.68	6.45E-01	7.64E-02	0.0578
6	2.86	7.37E-01	7.80E-02	0.0944
7	5.07	8.31E-01	9.36E-02	0.1252
8	7.22	9.11E-01	1.17E-01	0.1496
9	9.52	1.05E+00	1.52E-01	0.186
10	11.65	1.12E+00	1.59E-01	0.2175
11	13.85	1.20E+00	1.79E-01	0.2451
12	16.03	1.28E+00	2.17E-01	0.2729
13	18.08	1.31E+00	2.60E-01	0.2603

cir3_014.### from cir3014.OUT
9:14:46am on 9/22/92
Description 180 deg TE, no blowing
Comments No Problems
Barometric 28.9350
Re=499000
Cmu=0

Pt	Alp. corr.	Cl correct	Cd. corr.	WindCm
1	-8.33	-2.20E-02	5.47E-02	-0.099
2	-6.11	1.52E-01	5.81E-02	-0.0552
3	-3.79	3.56E-01	5.91E-02	-0.0242
4	-1.54	5.22E-01	6.83E-02	0.0147
5	0.69	6.38E-01	7.71E-02	0.0533
6	2.83	7.29E-01	7.56E-02	0.0902
7	5.09	8.35E-01	9.45E-02	0.1177
8	7.18	9.15E-01	1.17E-01	0.1399
9	9.46	1.03E+00	1.37E-01	0.176
10	11.66	1.13E+00	1.59E-01	0.2057
11	13.84	1.21E+00	1.72E-01	0.2332
12	16.02	1.28E+00	2.05E-01	0.2574
13	18.08	1.31E+00	2.40E-01	0.2697

cir3_005.### from cir3005.OUT
1:38:25pm on 9/17/92
Description Configuration 180 deg TE, 20 psig
Comments Model began shaking at 12 deg
Barometric 29.2070
Re=497000
Cmu=0.0555

Pt	Alp, corr.	Cl, correct	Cd, corr.	WindCm
1	-7.58	6.62E-01	1.64E-01	-0.1403
2	-5.31	8.27E-01	1.84E-01	-0.1028
3	-3.06	9.73E-01	2.08E-01	-0.0617
4	-0.84	1.11E+00	2.33E-01	-0.0222
5	1.36	1.24E+00	2.63E-01	0.0121
6	3.63	1.37E+00	3.01E-01	0.0478
7	5.87	1.47E+00	3.31E-01	0.0747
8	8.05	1.57E+00	3.76E-01	0.0993
9	10.28	1.68E+00	4.08E-01	0.1321
10	12.38	1.67E+00	4.35E-01	0.1678

cir3_006.### from cir3006.OUT
2:19:56pm on 9/17/92
Description Configuration 180 deg TE, 40 psig
Comments model shaking at last point
Barometric 29.1890
Re=496000
Cmu=0.156

Pt	Alp, corr.	Cl, correct	Cd, corr.	WindCm
1	-6.74	1.31E+00	5.92E-01	-0.1805
2	-4.43	1.46E+00	6.32E-01	-0.1421
3	-2.23	1.56E+00	6.62E-01	-0.1002
4	-0.02	1.72E+00	7.04E-01	-0.0666
5	2.18	1.82E+00	7.42E-01	-0.0309
6	4.5	1.98E+00	7.93E-01	0.001
7	6.75	2.07E+00	8.59E-01	0.0343
8	8.94	2.16E+00	9.02E-01	0.0557
9	11.18	2.29E+00	9.56E-01	0.0861
10	13.42	2.42E+00	1.02E+00	0.1144
11	15.65	2.51E+00	1.07E+00	0.1392
12	17.74	2.54E+00	1.12E+00	0.17

cir3_007.### from cir3007.OUT
2:59:59pm on 9/17/92
Description Configuration 180 deg TE, 60 psig
Comments No Problems
Barometric 29.1670
Re=495000
Cmu=0.260

Pt	Alp. corr.	Cl. correct	Cd. corr.	Wind Cm
1	-6.27	1.68E+00	1.11E+00	-0.2106
2	-4.02	1.84E+00	1.16E+00	-0.1748
3	-1.73	1.99E+00	1.20E+00	-0.1379
4	0.44	2.10E+00	1.25E+00	-0.101
5	2.76	2.28E+00	1.30E+00	-0.0711
6	5.06	2.39E+00	1.36E+00	-0.033
7	7.3	2.49E+00	1.43E+00	-0.008
8	9.47	2.57E+00	1.50E+00	0.0127
9	11.05	2.63E+00	1.53E+00	0.0351
10	13.96	2.80E+00	1.62E+00	0.0718
11	16.3	2.92E+00	1.70E+00	0.0966
12	18.37	3.02E+00	1.74E+00	0.1258
13	20.62	3.12E+00	1.82E+00	0.1451
14	22.73	3.17E+00	1.85E+00	0.1762

cir3_025.### from cir3025.OUT
10:30:11am on 9/23/92
Description Configuration 90 deg TE, no blo'
Comments No Problems
Barometric 29.4400
Re=467000
Cmu=0

Pt	Alp. corr.	Cl. correct	Cd. corr.
1	-8.37	-4.39E-02	6.26E-02
2	-6.11	1.26E-01	5.79E-02
3	-3.85	3.19E-01	5.63E-02
4	-1.59	5.01E-01	5.77E-02
5	0.58	6.29E-01	6.37E-02
6	2.74	7.31E-01	7.37E-02
7	4.89	8.28E-01	9.08E-02
8	7.04	9.05E-01	1.10E-01
9	9.15	1.01E+00	1.24E-01
10	11.32	1.12E+00	1.47E-01
11	13.59	1.22E+00	1.78E-01
12	15.69	1.28E+00	1.93E-01

cir3_008.### from cir3008.OUT
3:12:57pm on 9/18/92
Description Configuration 90 deg TE, 20 psig
Comments No Problems
Barometric 28.9470
Re=496000
Cmu=0.0669

Pt	Alp, corr.	Cl, correct	Cd, corr.	WindCm
1	-7.44	7.39E-01	1.91E-01	-0.1406
2	-5.13	9.12E-01	2.10E-01	-0.1041
3	-2.89	1.05E+00	2.36E-01	-0.0623
4	-0.64	1.22E+00	2.70E-01	-0.0262
5	1.57	1.34E+00	3.07E-01	0.0131
6	3.83	1.46E+00	3.42E-01	0.0487
7	6.08	1.57E+00	3.90E-01	0.0747
8	8.28	1.65E+00	4.35E-01	0.1012
9	10.48	1.77E+00	4.75E-01	0.1327
10	12.69	1.84E+00	5.16E-01	0.1681
11	13.72	1.83E+00	5.05E-01	0.1839

cir3_009.### from cir3009.OUT
2:01:55pm on 9/21/92
Description Configuration 90 deg TE, 30 psig
Comments No Problems
Barometric 28.9140
Re=499000
Cmu=0.112

Pt	Alp, corr.	Cl, correct	Cd, corr.	WindCm
1	-6.89	1.13E+00	3.59E-01	-0.1613
2	-4.65	1.26E+00	3.92E-01	-0.1249
3	-2.39	1.41E+00	4.21E-01	-0.0845
4	-0.17	1.55E+00	4.54E-01	-0.0485
5	2.06	1.67E+00	4.93E-01	-0.0123
6	4.35	1.79E+00	5.32E-01	0.0202
7	6.66	1.90E+00	5.82E-01	0.0525
8	8.82	2.02E+00	6.46E-01	0.0711
9	11.06	2.15E+00	6.99E-01	0.1066
10	13.29	2.26E+00	7.52E-01	0.1363
11	15.45	2.33E+00	7.89E-01	0.1644

cir3_010.### from cir3010.OUT
2:20:31pm on 9/21/92
Description Configuration 90 deg TE, 50 psig
Comments No Problems
Barometric 28.9070
Re=497000
Cmu=0.235

Pt	Alp. corr.	Cl, correct	Cd, corr.	WindCm
1	-6.28	1.59E+00	8.98E-01	-0.213
2	-4.02	1.73E+00	9.41E-01	-0.1748
3	-1.81	1.86E+00	9.88E-01	-0.1383
4	0.48	2.02E+00	1.05E+00	-0.1022
5	2.72	2.12E+00	1.10E+00	-0.0633
6	4.99	2.26E+00	1.17E+00	-0.0345
7	7.31	2.38E+00	1.24E+00	-0.0084
8	9.48	2.44E+00	1.30E+00	0.0177
9	11.71	2.58E+00	1.38E+00	0.0463
10	13.95	2.69E+00	1.44E+00	0.0773
11	16.17	2.79E+00	1.50E+00	0.1053
12	18.42	2.93E+00	1.59E+00	0.1319
13	20.66	3.00E+00	1.64E+00	0.159
14	22.77	3.07E+00	1.70E+00	0.1826

cir3_021.### from cir3021.OUT
8:43:33am on 9/23/92
Description Configuration 45 deg TE, No Blowing
Comments No Problems
Barometric 29.4240
Re=501000
Cmu=0

Pt	Alp. corr.	Cl, correct	Cd, corr.	WindCm
1	-6.38	-4.25E-02	5.44E-02	-0.0839
2	-6.13	1.15E-01	5.25E-02	-0.0394
3	-3.87	2.96E-01	4.78E-02	0.0174
4	-1.64	4.50E-01	4.81E-02	0.0688
5	0.50	5.65E-01	5.15E-02	0.1131
6	2.69	6.62E-01	5.72E-02	0.1542
7	4.82	7.53E-01	7.46E-02	0.1883
8	6.98	8.28E-01	8.94E-02	0.2135
9	9.13	9.38E-01	1.08E-01	0.2568
10	11.35	1.05E+00	1.34E-01	0.2953
11	13.55	1.14E+00	1.57E-01	0.329
12	15.66	1.23E+00	1.81E-01	0.3585
13	17.79	1.24E+00	2.05E-01	0.3714

cir3_019.### from cir3019.OUT
3:45:37pm on 9/22/92
Description Configuration 45 deg TE, 20 psig
Comments No Problems
Barometric 29.0300
Re=496000
Cmu=0.0726

Pt	Alp, corr.	Cl, correct	Cd, corr.	WindCm
1	-7.66	5.83E-01	1.48E-01	-0.055
2	-5.45	6.90E-01	1.63E-01	-0.0064
3	-3.23	8.20E-01	1.83E-01	0.045
4	-0.99	9.71E-01	2.04E-01	0.0952
5	1.24	1.16E+00	2.30E-01	0.1364
6	3.45	1.28E+00	2.58E-01	0.1814
7	5.65	1.37E+00	2.94E-01	0.2175
8	7.79	1.44E+00	3.21E-01	0.2505
9	10.01	1.56E+00	3.77E-01	0.2896
10	12.21	1.64E+00	3.87E-01	0.3321

cir3_022.### from cir3022.OUT
9:04:56am on 9/23/92
Description Configuration 45 deg TE, 30 psig
Comments No Problems
Barometric 29.4230
Re=502000
Cmu=0.123

Pt	Alp, corr.	Cl, correct	Cd, corr.	WindCm
1	-7.71	5.43E-01	2.87E-01	-0.056
2	-5.43	6.96E-01	3.02E-01	-0.0088
3	-3.2	8.64E-01	3.23E-01	0.043
4	-0.93	1.01E+00	3.38E-01	0.094
5	1.21	1.14E+00	3.68E-01	0.137
6	3.43	1.28E+00	3.96E-01	0.1827
7	5.64	1.37E+00	4.28E-01	0.219
8	7.8	1.48E+00	4.70E-01	0.2493
9	10.01	1.61E+00	5.09E-01	0.2939
10	12.25	1.74E+00	5.47E-01	0.3363
11	14.47	1.85E+00	5.89E-01	0.3755
12	16.58	1.92E+00	6.29E-01	0.4084

cir3_023.### from cir3023.OUT
9:22:42am on 9/23/92
Description Configuration 45 deg TE, 50 psig
Comments Ignore last point
Barometric 29.4240
Re=502000
Cmu=0.255

Pt	Alp, corr.	Cl, correct	Cd, corr.	WindCm
1	-7.47	7.09E-01	7.25E-01	-0.0625
2	-5.21	8.75E-01	7.47E-01	-0.0162
3	-3.03	9.77E-01	7.67E-01	0.0348
4	-0.75	1.18E+00	7.95E-01	0.0835
5	1.42	1.27E+00	8.23E-01	0.1311
6	3.59	1.41E+00	8.55E-01	0.1764
7	6.02	1.68E+00	9.22E-01	0.2117
8	8.22	1.78E+00	9.79E-01	0.2421
9	10.4	1.89E+00	1.02E+00	0.2869
10	12.62	2.03E+00	1.07E+00	0.3298
11	14.81	2.08E+00	1.11E+00	0.3725
12	17.13	2.31E+00	1.20E+00	0.4101
13	19.27	2.37E+00	1.24E+00	0.447
14	21.34	2.40E+00	1.26E+00	0.4848
15	23.48	2.48E+00	1.29E+00	0.5117

cir3_016.### from cir3016.OUT
12:38:17pm on 9/22/92
Description Similiar to Pelletier but Re=5*E5
Comments No Problems
Barometric 29.0120
Re=497000

Pt	Alp. corr.	Cl. correct	Cd. corr.	WindCm	Cmu
1	-8.37	-1.43E-02	6.03E-02	-0.097	0
2	-1.54	5.11E-01	7.17E-02	0.0165	0
3	5.1	8.44E-01	9.79E-02	0.1192	0
4	5.48	1.14E+00	1.65E-01	0.1001	0.0266
5	-1.21	7.92E-01	1.10E-01	0.0026	0.0266
6	-8	2.96E-01	7.58E-02	-0.1069	0.0266
7	-7.59	6.35E-01	1.84E-01	-0.1276	0.0677
8	-0.82	1.12E+00	2.39E-01	-0.0208	0.0677
9	5.87	1.50E+00	3.26E-01	0.0756	0.0677
10	6.25	1.78E+00	5.58E-01	0.0527	0.116
11	-0.46	1.39E+00	4.45E-01	-0.0406	0.116
12	-7.14	9.53E-01	3.71E-01	-0.1485	0.116
13	-6.84	1.19E+00	6.36E-01	-0.1689	0.177
14	-0.14	1.61E+00	7.21E-01	-0.0617	0.177
15	6.6	2.02E+00	8.65E-01	0.0298	0.177
16	6.83	2.20E+00	1.15E+00	0.0085	0.236
17	0.04	1.80E+00	1.01E+00	-0.0796	0.236
18	-6.67	1.36E+00	9.12E-01	-0.1856	0.236
19	-6.48	1.52E+00	1.21E+00	-0.2048	0.304
20	0.21	1.95E+00	1.31E+00	-0.0999	0.304
21	6.97	2.33E+00	1.48E+00	-0.0097	0.304

cir3_024.### from cir3024.OUT
10:01:28am on 9/23/92
Description 45 deg TE, repeatability chk of 21
Comments No Problems
Barometric 29.4600
Re=503000
Cmu=0

Pt	Alp. corr.	Cl correct	WindCd	WindCm
1	-3.37	-2.73E-02	5.23E-02	-0.0949
2	-1.64	4.58E-01	4.04E-02	0.0581
3	4.86	7.03E-01	6.90E-02	0.1893
4	11.36	1.04E+00	1.33E-01	0.2958

cir3_026.### from cir3026.OUT
11:21:36am on 9/23/92
Description hysteresis check, 180 deg TE, Cmu=0
Comments No Problems
Barometric 29.4520
Re=501000
Cmu=0

Pt	Alp. corr.	Cl. correct	WindCd	WindCm
1	13.79	1.21E+00	1.81E-01	0.2303
2	11.61	1.13E+00	1.59E-01	0.2053
3	9.37	1.01E+00	1.32E-01	0.1738
4	7.13	9.00E-01	1.06E-01	0.1431
5	5	8.23E-01	8.77E-02	0.1208
6	2.85	7.46E-01	8.80E-02	0.0939
7	0.63	6.18E-01	7.29E-02	0.0607
8	-1.57	4.89E-01	6.72E-02	0.0245
9	-3.83	3.12E-01	5.92E-02	-0.0125
10	-6.12	1.07E-01	6.19E-02	-0.0521
11	-8.38	-5.83E-02	7.05E-02	-0.0895

Reduced Pressure Data

Pressure Coefficient I
180 degree TE
Cmu=0
Alpha=0.69

X/C	Cp
0	0.827216
0.024	-0.69998
0.048	-0.83966
0.095	-0.97531
0.201	-0.84663
0.306	-0.85258
0.406	-0.79526
0.511	-0.73349
0.709	-0.69635
0.801	-0.65082
0.94	-0.17477
0.969	-0.178
0.991	-0.15902
1	-0.27731
0.991	-0.24057
0.969	-0.18688
0.94	-0.22927
0.902	-0.03711
0.804	0.057763
0.701	0.158688
0.604	0.123566
0.501	0.173221
0.403	0.181514
0.305	0.140521
0.203	0.026678
0.095	-0.03872
0.048	0.274146
0.017	0.575307
0	0.827216

Pressure Coefficient
180 degree TE
Cmu=0.26
Alpha=0.44

X/C	Cp
0	-0.07841
0.024	-2.01301
0.048	-1.89633
0.095	-1.9015
0.201	-1.52836
0.306	-1.31325
0.406	-1.47978
0.511	-1.48894
0.709	-1.80367
0.801	-2.27385
0.969	-8.00717
0.991	-11.2261
1	-8.41615
0.991	-1.62872
0.969	0.778982
0.94	0.772212
0.902	0.777788
0.804	0.74792
0.701	0.675841
0.604	0.591018
0.501	0.389912
0.403	0.566726
0.305	0.39469
0.203	0.489071
0.095	0.557965
0.048	0.757478
0.017	1.004779
0	-0.07841

Pressure Coefficient 90 deg TE Cmu=0.235 Alpha=0.40 degrees		Pressure Coefficient 45 degree TE Cmu=0.255 Alpha=-0.75	
X/C	Cp	X/C	Cp
0	-0.0376	0	0.283104
0.024	-2.04308	0.0223	-1.24048
0.048	-1.91995	0.0446	-1.2634
0.095	-1.95665	0.0883	-1.41051
0.201	-1.58116	0.1868	-1.18985
0.306	-1.54976	0.2845	-1.20943
0.406	-1.48616	0.3774	-1.18985
0.511	-1.50043	0.475	-1.13063
0.709	-1.82292	0.6591	-1.32884
0.801	-2.09323	0.7446	-1.44872
0.902	0.59393	0.8385	0.401075
0.804	0.59026	0.7474	0.357134
0.701	0.477327	0.6516	0.320358
0.604	0.468358	0.5615	0.320836
0.501	0.348901	0.4657	0.254925
0.403	0.516059	0.3746	0.241075
0.305	0.361948	0.2835	0.21194
0.203	0.449196	0.1887	0.217672
0.095	0.447157	0.0883	0.155582
0.048	0.719502	0.0446	0.341851
0.017	0.939253	0.0158	0.768358
0	-0.0376	0	0.283104

VITA

Captain John M. Tallarovic was born in Chicago, Illinois on May 10, 1966. He graduated from Saint Joseph High School in Westchester, IL in 1984 and attended the Illinois Institute of Technology, Chicago, IL. After graduation in 1988 with a Bachelor of Science degree in Mechanical and Aeronautical Engineering, he was commissioned through the Reserve Officer Training Corps program. He served as an aeronautical engineer at the Harry G. Armstrong Aerospace Medical Research Laboratory, Wright-Patterson Air Force Base, Ohio from January 1989 to May 1991

Permanent Address: 2440 South Lombard Avenue

Berwyn, Illinois 60402

REPORT DOCUMENTATION PAGE

Form Approved
OMB No. 0704-0188

1. AGENCY USE ONLY (Leave blank)	2. REPORT DATE December 1992	3. REPORT TYPE AND DATES COVERED Master's Thesis

4. TITLE AND SUBTITLE

An Experimental Investigation of a
Finite Circulation Control Wing

5. FUNDING NUMBERS

6. AUTHOR(S)

John M. Tallarovic, Captain, USAF

7. PERFORMING ORGANIZATION NAME(S) AND ADDRESS(ES)

Air Force Institute of Technology
Wright-Patterson AFB, OH 45433-6583

8. PERFORMING ORGANIZATION REPORT NUMBER

AFIT/GAE/ENY/92D-22

9. SPONSORING/MONITORING AGENCY NAME(S) AND ADDRESS(ES)

10. SPONSORING/MONITORING AGENCY REPORT NUMBER

11. SUPPLEMENTARY NOTES

12a. DISTRIBUTION/AVAILABILITY STATEMENT

Approved for public release; distribution
unlimited

12b. DISTRIBUTION CODE

13. ABSTRACT (Maximum 200 words)

This wind tunnel investigation examined the lift, drag, and pitching
moment of a 20% thick, 8.5% camber, partial elliptical cross-section,
single blowing slot, rectangular, circulation control wing. The
aspect ratios tested were 3.71 and 3.99. Variables included three
differently shaped trailing edge Coanda surfaces and steady blowing
and pulsed blowing. The test Reynolds number, based on the chord
was 500,000. The angle of attack was varied from minus 6 degrees
to the inception of stall. The maximum lift coefficient measured
was 3.17 with an equivalent drag coefficient of 1.85. Results also
show a limit to increasing lift by increasing the blowing.
Additionally, a 90 degree Coanda surface had equal lift performance
and better drag performance than a 180 degree Coanda surface.

14. SUBJECT TERMS

Circulation Control, V/STOL Aircraft
Wind Tunnel Testing, Wing, Pulsed Blowing

15. NUMBER OF PAGES
64

16. PRICE CODE

17. SECURITY CLASSIFICATION OF REPORT	18. SECURITY CLASSIFICATION OF THIS PAGE	19. SECURITY CLASSIFICATION OF ABSTRACT	20. LIMITATION OF ABSTRACT
Unclassified	Unclassified	Unclassified	UL